# Threading the biophysics of mammalian Slo1 channels onto structures of an invertebrate Slo1 channel

Yu Zhou,[1]* Huanghe Yang,[3]* Jianmin Cui,[2] and Christopher J. Lingle[1]

[1]Department of Anesthesiology, Washington University School of Medicine, St. Louis MO
[2]Department of Biomedical Engineering, Washington University, St. Louis, MO
[3]Department of Biochemistry, Duke University School of Medicine, Durham, NC

For those interested in the machinery of ion channel gating, the $Ca^{2+}$ and voltage-activated BK $K^+$ channel provides a compelling topic for investigation, by virtue of its dual allosteric regulation by both voltage and intracellular $Ca^{2+}$ and because its large-single channel conductance facilitates detailed kinetic analysis. Over the years, biophysical analyses have illuminated details of the allosteric regulation of BK channels and revealed insights into the mechanism of BK gating, e.g., inner cavity size and accessibility and voltage sensor-pore coupling. Now the publication of two structures of an *Aplysia californica* BK channel—one liganded and one metal free—promises to reinvigorate functional studies and interpretation of biophysical results. The new structures confirm some of the previous functional inferences but also suggest new perspectives regarding cooperativity between $Ca^{2+}$-binding sites and the relationship between voltage- and $Ca^{2+}$-dependent gating. Here we consider the extent to which the two structures explain previous functional data on pore-domain properties, voltage-sensor motions, and divalent cation binding and activation of the channel.

## Introduction

Despite the ability of ion channel biophysics to provide insightful inferences regarding structural features of a given ion channel, those invested in biophysical approaches eagerly await each advance in structural information, hoping to gain clarity or validation regarding functional questions or to identify new directions to better probe and understand function. One such channel for which detailed structural information has been long awaited is the large-conductance, voltage- and $Ca^{2+}$-activated $K^+$ channel (Slo1 or BK, the pore-forming subunit encoded by the *kcnma1* gene). For biophysicists, the Slo1 channel has been a particularly tantalizing subject. First, the large single-channel conductance of the Slo1 channel seductively enabled the robust application of detailed single-channel analysis to Slo1 gating properties. Second, the dual regulation by both membrane voltage and cytosolic $Ca^{2+}$ posed the intriguing problem of how two distinct physiological stimuli might interact to favor channel activation. Third, over the years, several aspects of Slo1 channel function have exhibited features that were not clearly reconcilable with comparable studies on voltage-dependent $K^+$ (Kv) channels, even though they share relatively homologous S1–S6 voltage-sensing and pore domains. Thus, to help understand the unique functional features of Slo1 channels, full structural information has been eagerly awaited.

Now, using cryo-electron microscopy, the MacKinnon laboratory has provided two structures of a full-length *Aplysia californica* Slo1 (aSlo1) channel, one a $Mg^{2+}$/$Ca^{2+}$ liganded conformation (Tao et al., 2017) and the other an EDTA-treated, metal-free conformation (Hite et al., 2017). The results present some surprises and new insights, some confirmations, and some challenges to previous inferences. The new structures provide guidance pertinent to a large number of functional studies done over the years. Our intent here is to highlight to what extent various functional results are either consistent or inconsistent with the new structures. When the biophysics seems inconsistent with the structures, we attempt to assess how this may be reconciled. Despite the plethora of detailed biophysics that has been brought to bear on mammalian Slo1 channels, the availability of the aSlo1 structures is certain to spawn much additional new work seeking to tease apart the underlying mechanisms of Slo1 channel gating. For simplicity, we use "liganded" and "metal-free" to describe the two aSlo1 structures. Readers should keep in mind two cautionary remarks in regard to this discussion. First, many readers may assume that "liganded" and "metal-free" structures correspond to "open" and "closed," but the authors are notably judicious about the functional correlates of these two structures. Some topics addressed here speak to the question of whether a given structure exhibits features likely to be consistent with a given functional state, i.e., open or closed. Second, the *Aplysia* Slo1 protein

*Y. Zhou and H. Yang contributed equally to this paper.
Correspondence to Jianmin Cui: jcui@wustl.edu; Christopher J. Lingle: clingle@morpheus.wustl.edu

Abbreviations used: bbTBA, *N*-(4-[benzoyl]benzyl)-*N*,*N*,*N*-tributylammonium; CTD, cytosolic domain; Kv channel, voltage-dependent $K^+$ channel; MthK, $K^+$ channel from *Methanobacterium thermoautotrophicum*; MTSET, 2-(trimethylammonium) ethyl MTS; PGD, pore-gate domain; Po, open probability; RCK, regulator of conductance for $K^+$; TM, transmembrane; VSD, voltage-sensing domain.



The Rockefeller University Press
J. Gen. Physiol. 2017 Vol. 149 No. 11 985–1007
https://doi.org/10.1085/jgp.201711845

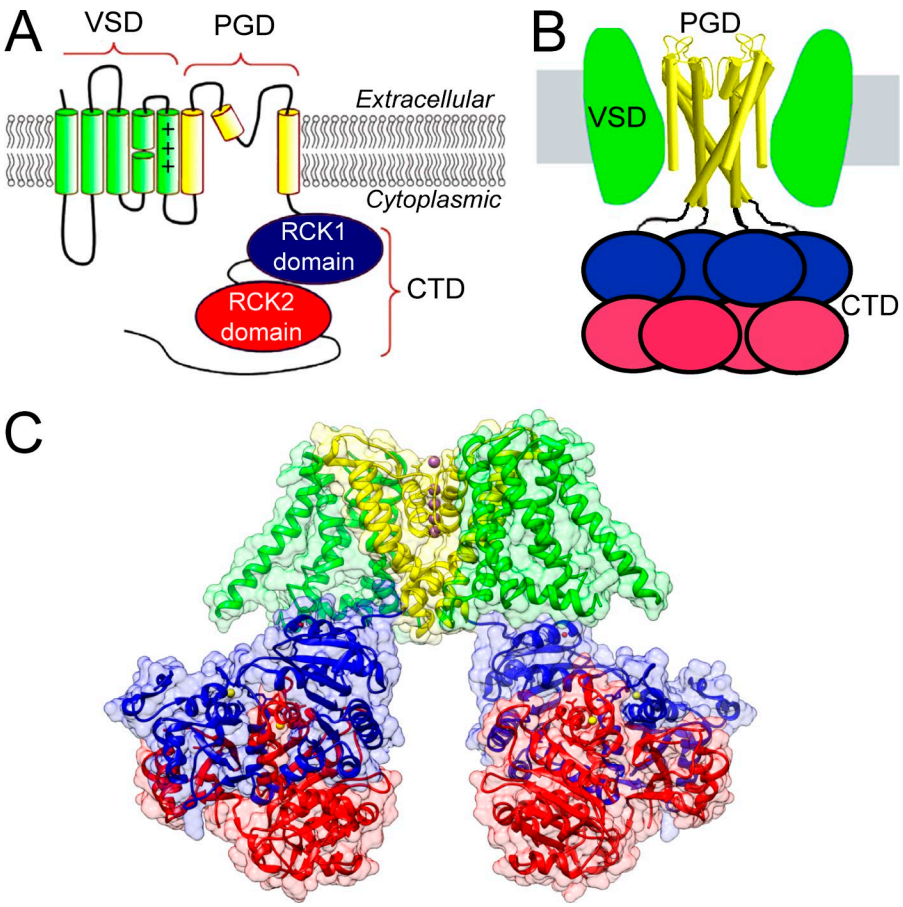


Figure 1. **Components of a Slo1 α subunit and Slo1 channel.** (A) Topology map of a single pore-forming Slo1 α subunit highlighting its three distinct domains, PGD (S5-pore loop-S6), VSD (S0–S4), and CTD (two RCK domains per subunit; Rothberg, 2012). (B) Schematic of modular origin of a Slo1 channel highlighting the octameric arrangement of RCK domains in the CTD. (C) Color-coded map of PGD (yellow), VSD (green), and CTD (red, RCK2; blue, RCK1) in the liganded aSlo1 structure. $Ca^{2+}$ ions are yellow spheres, $Mg^{2+}$ ions are red spheres, and $K^+$ ions are purple spheres.

does not exhibit uniform sequence conservation with mSlo1. As such, one must keep in mind the possibility that some aspects of aSlo1 may not be good correlates of mSlo1. This is examined in more detail in this review. Despite such considerations, the new structures permit a new level of evaluation of Slo1 function.

The overall architecture of Slo1 channels follows a modular design (Fig. 1). Each pore-forming α subunit (Fig. 1 A) in the Slo1 tetramer (Yang and Cui, 2015) contains a set of transmembrane helices, which define two functional elements: first, the ion conducting part of the channel (S5–S6), termed the pore-gate domain (PGD), and second, the S0–S4 voltage-sensing domain (VSD). Together, the S1–S6 transmembrane helices in the PGD and VSD are homologous to those in Kv channels, with an additional S0 helix in Slo1 that attaches to the VSD. Appended to the membrane-associated elements of the subunit is an extended sequence that extends into the cytosol (Fig. 1 A). When assembled in a full tetramer (Fig. 1 B), the Slo1 channel contains three distinct domains: (1) the ion-conducting PGD, (2) the VSD, and (3) a ligand-sensing cytosolic domain (CTD). The modular design suggests that each individual module may undergo relatively independent conformational changes in response to corresponding stimuli, while also enabling allosteric coupling through extensive protein–protein interactions. Structural studies guiding Slo1 channel work began with x-ray crystallographic images of intracellular C-terminal domains of prokaryotic $K^+$ channels, which defined so-called regulator of conductance for $K^+$ (RCK) domains (Jiang et al., 2001, 2002a,b). These papers revealed that RCK domains in both an *Escherichia coli* 6TM $K^+$ channel and a $K^+$ channel from *Methanobacterium thermoautotrophicum* (MthK) contained ligand-binding sites likely to be important in channel regulation, and furthermore, that such domains shared homology with similar RCK domains in Slo1 (Fig. 1 B). Thus these prokaryotic channel structures provided a structural framework for the mutational work that established that the RCK1 and RCK2 domains in mouse Slo1 (mSlo1) each contain distinct divalent cation regulatory sites, which together account for all direct $Ca^{2+}$-dependent activation by physiological concentrations of $Ca^{2+}$ (Schreiber and Salkoff, 1997; Shi et al., 2002; Xia et al., 2002; Sweet and Cox, 2008; Zhang et al., 2010).

The recent structures of full-length aSlo1 (e.g., Fig. 1 C), by providing detailed views of the membrane-spanning elements (including PGD and VSDs) in association with CTD, now allow more directed focus on questions central to understanding mechanisms of gating. In the following discussion, we consider three

general areas: (1) topics pertinent to the permeation pathway and PGD; (2) topics related to ligand sensing and the gating ring defined by the CTD; and (3) topics having to do with the VSD. We approach these areas by first summarizing the functional data and then assessing to what extent they may be consistent with the structures. We conclude that there is satisfying congruence between many of the inferences obtained from biophysical studies and the new structures, particularly in regard to determinants of regulation by $Ca^{2+}$ and $Mg^{2+}$, the large size of the inner cavity, and also modest voltage-dependence of activation. In addition, the new structures highlight some unanticipated features that have functional implications, e.g., the importance of interfaces between the PGD and the CTD in coupling of ligand-binding to activation, and also the role of cooperativity in $Ca^{2+}$-dependent activation.

### aSlo1 as a model for mammalian Slo1

Given that biophysical studies on Slo1 channels have largely focused on mammalian forms, based on evolutionary considerations one must consider whether the aSlo1 structure will be fully generalizable to its mammalian counterpart. The closest homologue of the mSlo1 channel is, in fact, the sperm-specific pH-regulated Slo3 channel (Schreiber et al., 1998). Divergence between *Aplysia* and mammalian Slo1 genes began far before the gene duplication that resulted in Slo3. Although selective pressures on a channel playing the functional roles served by Slo1 may preserve particular functional attributes between mSlo1 and aSlo1, which nature has not preserved in Slo3, it is useful to consider the extent of conservation among these three channels. Comparison of residue identities among mouse and human Slo1, aSlo1, and mouse and human Slo3 (Fig. 2 A) shows that mammalian Slo1 and aSlo1 share the highest fraction of identical residues in the portion of RCK1 involved in ligand recognition (Fig. 2 C) and also in a segment that includes the $Ca^{2+}$ bowl (Fig. 2 D). Conservation in the membrane-associated portions of mammalian Slo1 and aSlo1 are much weaker (Fig. 2, A and B) and, in the pore-lining S6, mammalian Slo1 is more similar to Slo3 than to aSlo1. aSlo1, in fact, contains a large number of residues unique to it in several different transmembrane (TM) segments, including S0, the more cytosolic portion of S4, and also throughout S5 and S6. Although some of these amino acid changes may be highly conservative, they do raise the possibility that there are functional differences that have developed over time. Pertinent to this idea, Slo1 channels in a marine organism such as *Aplysia* may have been subjected to different selective pressures than those in mammals. For example, seawater and the hemolymph of most marine animals contain ~50 mM $Mg^{2+}$ (Prosser, 1973), whereas the free intracellular $Mg^{2+}$ concentration may exceed 5 mM (Brinley et al., 1977), clearly higher than in mammals. Given these considerations, it would not be surprising if some details of function and structure may differ between aSlo1 and mammalian Slo1. Yet, the strong conservation and even extensive residue identity, particularly throughout the CTD, make the aSlo1 a compelling model for consideration of the extent to which the new structural data aligns with previous biophysical results.

### The Slo1 pore-gate domain

Several independent functional studies have converged on the view that some structural features of the Slo1 S6 and inner cavity may differ substantially from those of their Kv channel relatives. This has included the dimensions of the inner cavity, in both open and closed conditions, whether particular residues may be pore-facing or buried, the state-dependent accessibility of S6 residues, the location of any gate to permeation, and what changes in S6 may occur during gating. Although the amino acid similarity between mSlo1 and aSlo1 is lowest in the TM portion of these proteins, it is valuable to assess whether the new structures may provide insight into the functional results and vice versa. Do the structures support the functional distinctions observed between Slo1 and Kv channels?

**The open Slo1 inner cavity has an unusually large diameter.** Functional studies have suggested that the Slo1 inner cavity may be unusually large, compared with other eukaryotic $K^+$ channels, even at positions in S6 likely to be close to the entrance to the selectivity filter. The evidence includes (1) rapid inhibition by relatively large molecules that block from the cytosolic side of the channel (Li and Aldrich, 2004), (2) the ability of some molecules perhaps too large to inhibit Kv channels to inhibit Slo1 channels (Wilkens and Aldrich, 2006; Tang et al., 2009), (3) the ability of MTS reagents, including the very bulky Texas Red–2-aminoethyl MTS hydrobromide (MTSEA), to modify cysteine residues introduced at positions deep in the inner cavity (Zhou et al., 2011), and (4) the effects of bulk sugars (Brelidze and Magleby, 2005) and changes in side-chain volume of amino acids at the entrance to the inner cavity (Geng et al., 2011) on single-channel conductance. The latter study calculated an effective radius at the entrance to the inner cavity of 8–10 Å, consistent with the calculated dimensions of the liganded aSlo1 structure (Fig. 3 A). Together, these results support the idea that the liganded aSlo1 structure, assumed to be open, exhibits a larger inner cavity radius than Kv channels (Fig. 3 A, as typified by KvChim, a chimeric Kv channel in which the voltage-sensor paddle has been transferred from Kv2.1 to Kv1.2). At a position just after the cytosolic end of Slo1 S6 (aK317/mN328; note that throughout we use the prefix "a" to denote residues in the *Aplysia* sequence and "m" to indicate the corresponding mammalian res-

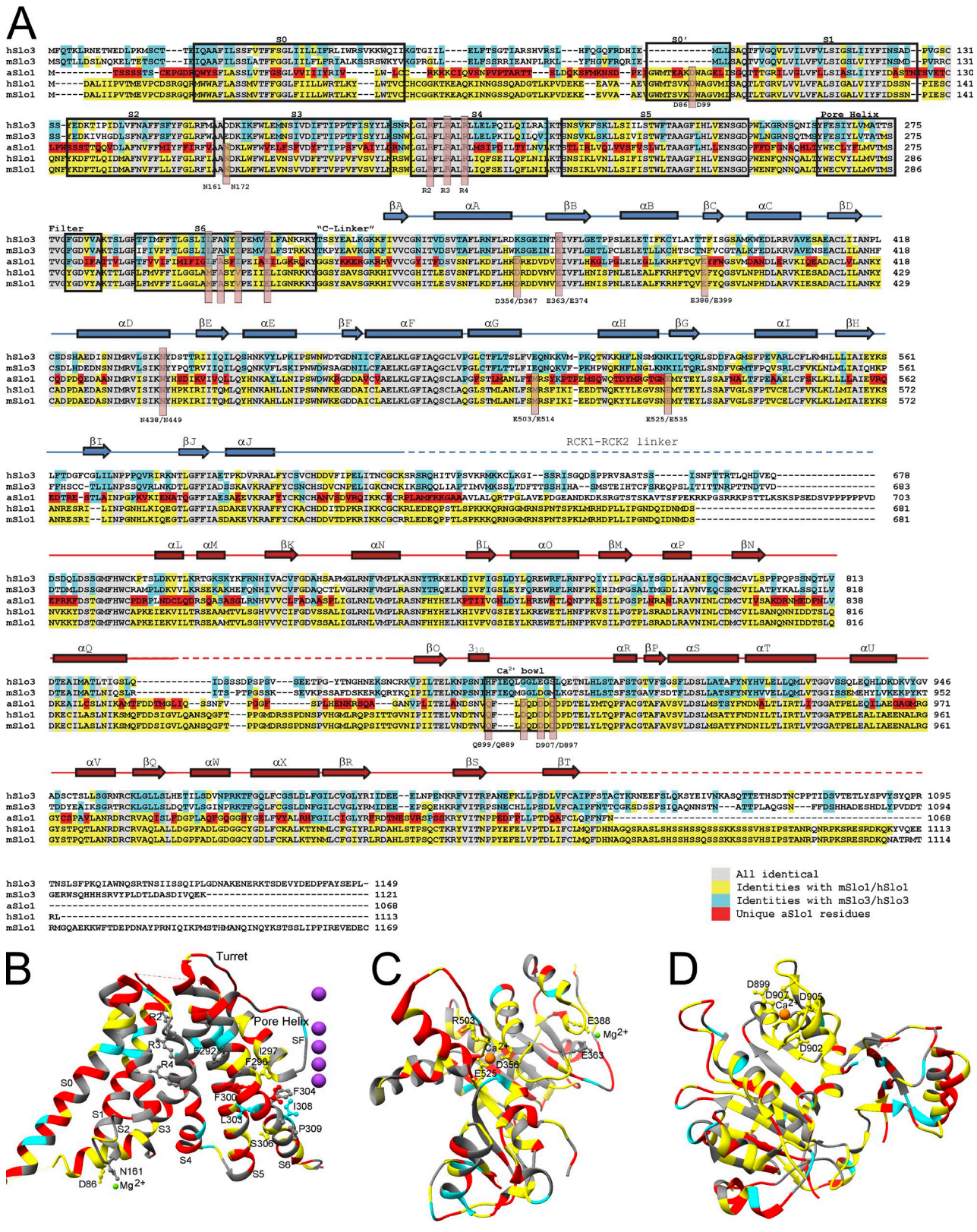


Figure 2. **Residue conservation among Slo family members.** (A) *Aplysia* (aSlo1) sequence is compared with human and mouse Slo3 and Slo1. Residues identical in all species are gray; mammalian Slo1 residues shared with aSlo1 and perhaps one Slo3 sequence are in yellow; residues shared with Slo3 are in cyan; residues unique to aSlo1 are in red. Note the strong conservation of aSlo1 with mSlo1 through the first part of RCK1 and also surrounding the $Ca^{2+}$ bowl region. In S0–S6, many more residues unique to aSlo1 are found, most notably more cytosolic part of S4 and also much of S5 and S6. Much of aSlo1 S0 is also poorly conserved. (B) The same color coding is mapped onto the *Aplysia* liganded S0–S6 structure, again highlighting the large number of residues unique

idue), the liganded structure approaches a pore radius of ~10 Å. On balance, the dimensions of the liganded aSlo1 structure match well with the predictions from functional experiments.

Intriguingly, the differences in inner cavity radius between the liganded and metal-free aSlo1 structures are surprisingly small (Fig. 3 A). This contrasts with differences between a presumably closed KcsA (1K4C) and open KvChim (2R9R) structures (Fig. 3, B, D, and F), and similar differences between closed and open Kv1.2 are also observed (Pathak et al., 2007). As the Slo1 inner cavity narrows toward the selectivity filter, at residue aA305 (mA316), a position at which modification of introduced cysteines by 2-(trimethylammonium) ethyl MTS (MTSET) can occur (Zhou et al., 2011), the inner cavity radius still exceeds 5 Å, before tapering substantially as the selectivity filter is approached. The pore dimensions of aSlo1 and KvChim are grossly similar in these deeper parts of the inner cavity (aI299-aA305/mG310-mA316), with the wider entryway to the inner cavity of aSlo1 only beginning to be apparent at a position (aF309-aE313/mY318-mE324) corresponding to the PVP motif in Kv channels. At the approximate position of aE313 (mE324), the liganded aSlo1 inner cavity has expanded to a radius of ~8 Å (Fig. 3 A), whereas the presumably open KvChim retains an inner cavity radius of less than 5 Å (Fig. 3, A and B). The difference in dimensions between the open KvChim and liganded aSlo1, particularly at the entryway to the inner cavity, seem consistent with differences in blocker access to the open channel and the estimates of pore dimensions based on biophysical inferences.

Accessibility of the inner cavity in closed states. Slo1 channels also differ from Kv channels in regard to whether bulky blocking molecules may access and occupy the central cavity even in closed states. Inhibition of Slo1 channels by *N*-(4-[benzoyl]benzyl)-*N*,*N*,*N*-tributylammonium (bbTBA), a large quaternary ammonium blocker, shows features such as unaltered deactivation kinetics and three exponential components during current inhibition, which are inconsistent with simple open channel block. Rather, the results are best explained by perturbation of the equilibrium between inhibition of both closed and open states as channels are activated (Li and Aldrich, 2004). On the other hand, examination of Slo1 channel inhibition by a modified *Shaker* ball peptide (EBP) reveals that this bulky inhibitor delays channel closing during recovery from block. Furthermore, the time dependence in EBP inhibition supports a true state dependence of EBP inhibition. Together, these results indicate that there is a conformational change at the cytosolic end of the Slo1 channel that controls access of at least large molecules to the central cavity (Li and Aldrich, 2004). In addition, an analysis of the ability of bbTBA to inhibit Slo1 channels under conditions where voltage-sensors are entirely in resting states suggested that bbTBA is unlikely to block Slo1 channels in fully resting states with four inactive voltage-sensors, but that voltage-dependent conformational changes preceding channel opening were permissive for bbTBA inhibition (Tang et al., 2009). Although one might argue that a change in inhibition by bbTBA reflects not a change in accessibility, but a change in affinity, such that perhaps bbTBA can access the inner cavity in a fully closed conformation, but that binding affinity is simply much weaker, it is difficult to imagine that there should be such a bulk change in hydrophobicity within the inner cavity upon activation. On balance, the functional studies suggest that, like Kv channels, there are conformational changes at the cytosolic end of the Slo1 S6 helices, but, even in some nonconducting states, compounds can enter and exit the Slo1 central cavity. However, there may be a set of closed states, perhaps dependent on the status of the voltage-sensors, that differ in the extent to which larger compounds can access the inner cavity.

How do these results accord with the new structural information? The two aSlo1 structures reveal only minor differences in the dimensions of the inner cavity (Fig. 3 A). In fact, a molecule of the dimensions of bbTBA can be readily accommodated within the inner cavity of both aSlo1 structures (Fig. 3 C), although the exact position of occupancy by bbTBA might vary slightly between structures. In contrast, bbTBA appears to be unable to access the Kv inner cavity based on the KvChim structure (Fig. 3 D). What about *Shaker* EBP access? Docking of the first 10 residues of an α-helical conformation of the *Shaker* EBP suggests that it may readily access and occupy the aSlo1 inner cavity in both liganded and metal-free structures (Fig. 3 E), which contrasts with the state dependence of functional inhibition. For comparison, the same *Shaker* EBP conformation appears unable to penetrate fully into the KvChim inner cavity without adopting a random coil (Fig. 3 F).

Although the aSlo1 structures seem in accord with the bbTBA functional results, the absence of any restriction to Shaker EBP access in the metal-free state seems at variance with the functional data. One possibility is the metal-free structures, despite the presence of EDTA,

to aSlo1. Important residues shared among Slo3, aSlo1, and mammalian Slo1 include mR207, mR210, and mR213. (C) Extent of conservation is mapped onto the RCK1 domain. In this case, aSlo1 shares strong identity with much of the mammalian sequences in the vicinity of the ligand-binding structures. (D) Elements of RCK2 near the $Ca^{2+}$ bowl motif are highly conserved between aSlo1 and mammalian Slo1.

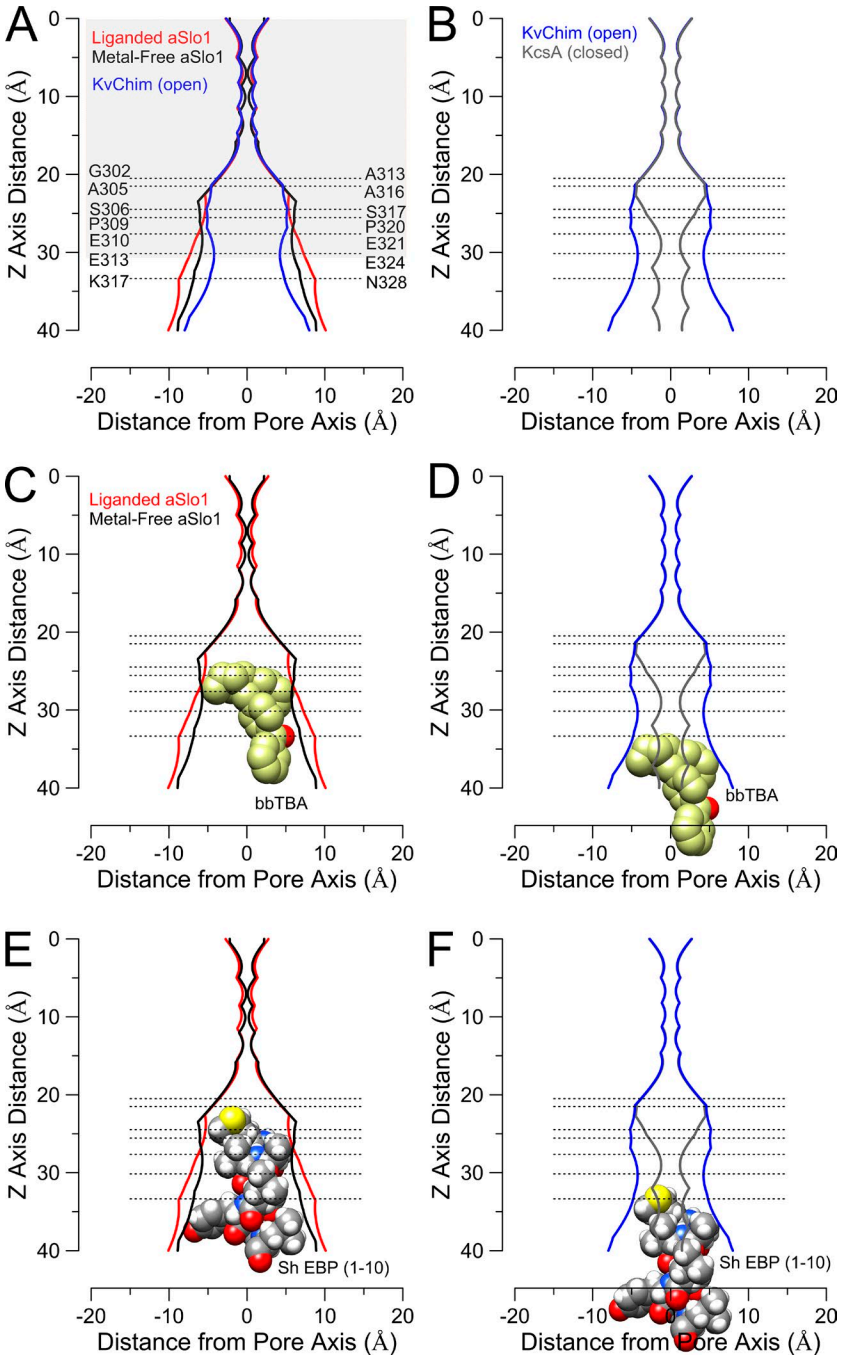


Figure 3. **Pore dimensions of aSlo1 channels accommodate large blockers.** (A) Pore radius for liganded and metal free *Aplysia* Slo1 structures along with the open KvChim structure are compared. Residue numbering corresponds to *Aplysia* on left and mammalian Slo1 on right. Shaded area corresponds approximately to the lipid bilayer dimensions. (B, D, and F) The open KvChim pore is compared with the closed KscA pore. The open KvChim structure is used here because it contains an attached VSD domain. (C) bbTBA can be accommodated deep in the inner cavity in both liganded and metal-free aSlo1 structures. Here and in D, the bbTBA orientation was constrained to place the quaternary group as close as possible to the observed position of TEA occupancy in KcsA (Lenaeus et al., 2005). (D) bbTBA is unlikely to penetrate deeply into an open KvChim pore. (E) An α-helical conformation of the 10 N-terminal residues of the *Shaker* extended ball peptide can be docked in both the liganded and metal-free aSlo1 structures. Blocker orientation was chosen to allow deepest penetration. (F) The *Shaker* EBP in a compact helical structure would be unlikely to penetrate deeply into a KvChim-like pore, without adopting a random coil.

may differ from a fully closed Slo1 channel, perhaps reflecting partially activated, but yet nonconducting states, as has been proposed to account for closed-state inhibition by bbTBA (Tang et al., 2009). Alternatively, there may be structural differences between *Aplysia* and mammalian Slo1 in the PGD, perhaps reflecting the weaker sequence conservation in this region compared with other domains of the channel. Finally, there is the possibility that the determinants of binding affinity for both peptides and bulky hydrophobic blockers may differ between closed and open states, even though compounds can still gain access to the inner cavity. In the latter case, there is no obvious change in inner cavity hydrophobicity that might account for this. Irrespective of whether large molecules are able to enter the Slo1 inner cavity in particular functional states, both the functional results and structural data suggest that the permeant ion, $K^+$, can readily enter and exit the inner cavity in all functional states.

**Where is the Slo1 channel permeation gate?** The absence of any appreciable constriction to inner cavity access in the metal-free aSlo1 structure naturally raises a question about where the physical gate to ion perme-

ation resides. The permeation gate of any ion channel represents that part of the channel that provides the barrier to ion permeation in the closed state. This is typically assumed to involve a physical block or narrowing, although other physico-chemical mechanisms, perhaps arising from wetting-dewetting within the confines of a narrow hydrophobic pathway, may exist (Roth et al., 2008; Aryal et al., 2014). For Slo1 and other members of the Slo family of channels, identification of the gate remains incompletely resolved. For Kv channels, in the closed state a crossing of inner pore M2/S6 helices at the cytosolic end of the inner cavity prevents ion access to the inner cavity (Liu et al., 1997; Doyle et al., 1998; del Camino and Yellen, 2001). Yet for other $K^+$ channels, functional data suggest that an impediment at the cytosolic end of S6 that prevents ion access to the inner cavity is not present. This includes the MthK channel (Posson et al., 2013, 2015), cyclic nucleotide-gated channels (Contreras et al., 2008), the KCNT2.2 Slo2.2 $Na^+$-activated $K^+$ channel (Garg et al., 2013), and the $Ca^{2+}$-activated, but voltage-independent, small-conductance $K^+$ channel (Bruening-Wright et al., 2002). Similarly, Slo1 channels have been included in this group (Wilkens and Aldrich, 2006; Zhou et al., 2011, 2015; Thompson and Begenisich, 2012). Two main approaches have been brought to bear on this question. First, the state dependence of action of cytosolic channel blockers has been used to make inferences about inner cavity accessibility. Second, the idea that a gate to permeation is not present at the cytosolic end of a channel has also been tested by the use of various probes, such as MTS reagents or metals such as $Ag^+$ or $Cd^{2+}$, that react with cysteines introduced into S6. Cysteine-reactivity is then measured under conditions that strongly favor either open or closed states, to allow determination of the state-dependence of modification.

For Slo1 channels, the functional tests argue that the inner cavity can be accessed by both small (Zhou et al., 2015) and larger (Li and Aldrich, 2004; Wilkens and Aldrich, 2006; Tang et al., 2009) molecules under conditions where channels are nonconducting. Furthermore, deep pore residues (residues above the canonical YVP/PVP motif in mSlo1/Kv channels), when substituted with cysteine, can be modified in closed states much more readily than in *Shaker* (Zhou et al., 2011). However, Slo1 channels do appear to share with other $K^+$ channels a conformational change at the cytosolic end, as indicated by the state dependence of inhibition by Shaker EBP (Li and Aldrich, 2006). So, if there is an aperture at the cytosolic end of Slo1 S6 that permits access of small molecules to the inner cavity in closed states, where is the actual gate that limits ion permeation? The new structures provide limited insight into this question, and the authors choose to leave this question open (Hite et al., 2017). Although the term "selectivity filter gate" has become commonly used, comparison of the selectivity filter region of all available $K^+$ channel structures has failed to identify any clear difference among those structures thought to be in closed states and those thought to be in open states. Thus, the question of the location of the Slo1 gate remains unresolved. Given that the two aSlo1 structures reveal no basis for difference in access, even for the Shaker EBP, whereas the functional tests of MTS accessibility and both Shaker EBP and bbTBA access imply some state dependence, again it must be considered that the metal-free structure represents an already partially activated conformation.

Conformational changes in Slo1 S6 during activation. Mutational studies have sought to make inferences about S6 conformational changes based on the ability of side-chain substitutions to influence the Slo1 gating range. The key idea is that, if a side-chain undergoes a change in solvent accessibility during gating, e.g., moving from partially buried to fully exposed in the aqueous milieu, the energetic preference of that side-chain for a given environment may favor a particular functional state. For mSlo1, two distinct types of tests have suggested that some or all of residues mL312, mA313, mA316, and mS317 (aI301, aG302, aA305, and aS306) undergo changes in environment during gating.

In one approach, the behavior of mSlo1 S6 residues during gating was probed by systematic introduction of charged or protonatable residues in S6 (Chen and Aldrich, 2011; Chen et al., 2014). Although several S6 positions influence gating shifts, interesting deep pore positions were mL312, mA313, and mA316 (Chen et al., 2014). Irrespective of whether D or K was substituted in positions mL312, mA313, or mA316, each mutation resulted in constitutively open channels. Position mM314, when mutated to a protonatable residue, also results in pH-dependent leftward-shifted gating at low pH (Chen and Aldrich, 2011). Similarly, when mA313 is replaced by cysteine, MTSET modification at this position also results in essentially constitutively active channels (Zhou et al., 2011). For mA316C, MTSET modification results in marked inhibition of Slo1 currents, precluding assessment of gating shifts, whereas mL312C is essentially constitutively open even without modification. All of these results were explained by the idea that side chains at these positions are more likely to be exposed to the aqueous milieu when the channel is open.

The modification of cysteines substituted for deep pore residues in mSlo1 have also suggested some potential differences between S6 in Slo1 and that in Kv channels, specifically *Shaker*. The modification by MTS ET of deep pore mSlo1 S6 positions, A313C, A316C, and S317C, are homologous to positions in *Shaker* that were not modified in similar studies (Liu et al., 1997). Furthermore, although the rates of modification in open states at these deep pore positions were ~2-3 orders of magnitude faster than closed states, closed state

modification did occur at rates at least another 2 orders of magnitude faster than observed in *Shaker* (where essentially no closed state modification of deep pore residues is observed). As discussed in the previous section (Accessibility of the inner cavity in closed states), based on the idea that large inhibitory molecules can access the inner cavity of mSlo1 channels, the differences in modification rates between closed and open conditions might reflect the possibility that side chains at positions mA313, mA316, and mS317 may become more exposed to solvent upon opening, perhaps involving rotation of the S6 helix (Chen et al., 2014), an interpretation also supported by the large leftward gating shift after MTS modification of mA313C (Zhou et al., 2011). To account for the differences in patterns of MTS modification of residues between mSlo1 and *Shaker*, it was suggested that pore-facing (accessible) residues in mSlo1 do not align with those in *Shaker*, perhaps reflecting the influence of the unique diglycine motif in mSlo1 (G310/G311) on the continuity of the α-helix in mSlo1 S6.

Do the new structures provide any insight into these functional results, i.e., the effect of charged residues in the deep inner cavity, the consequences of MTS modification of introduced cysteines, and the differences in pattern of MTS modification between mSlo1 and *Shaker*? Given the modest changes in pore radius between the metal-free and liganded aSlo1 structures, major changes in S6 properties do not seem obvious. To provide a gross overview of changes between structures in S6, we created morphs between the metal-free and liganded aSlo1 structures using the selectivity filter and pore helix to anchor the structural alignments (Video 1, Slo1 pore-axis view; Video 2, Slo1 side view) and also created similar morphs for Kv1.2 closed and open states generated computationally via the Rosetta-Membrane method and molecular dynamics simulations (Pathak et al., 2007; Video 3, Kv1.2 pore-axis view; Video 4, Kv1.2 side view) Although such morphs can involve physically implausible trajectories of motion (i.e., steric clashes in space-filling models), they can serve as useful visual guides to the changes in positions and orientations that may occur between pairs of structures. Details are provided in the legends. For Slo1, two gross features are apparent. First, in the view from the cytosol, the Slo1 S6 helices define an apparent "square," which is retained during "gating," with each S6 helix being pulled along the side of the square. Second, although there is a small clockwise rotation of the S6 helix, particularly toward the cytosolic end of S6, there appears to be little obvious change in orientation of any residue that might be expected to account for any state-dependent accessibility or influence on gating. For Kv1.2, although the S6 helices again define an initial square, during the change to an open conformation, the S6 helices move outward to increase the central cavity dimensions in a classic blooming flower fashion. These S6 motions represent a major difference between the Slo1 and Kv. For Slo1, the lateral motion of S6 across the pore axis produces little expansion of the inner cavity, whereas in Kv the outward movement of the S6 helixes dramatically increases the dimensions of the inner cavity. The basis for such differences may arise from differences between Kv and BK channels in regard to the organization of the VSD and PGD domains, discussed in more detail later.

To provide additional guidance that might help explain functional data, we undertook some *ad hoc* measures of S6 properties. It is useful to keep in mind that the orientations of the side chains in these structures, particularly in the metal-free structure, are of fairly low resolution, leading us to focus primarily on aspects of the S6 helix and Cα carbon positions. To examine the potential movement of Cα carbons between structures, we measured the angular change in the vector between diagonally opposed Cα carbons as illustrated for position aP309 (Fig. 4 A). Beginning near aI299/aF300 (mG310/mG311), each Cα carbon is rotated counterclockwise around the pore axis in the liganded structure (red symbols in Fig. 4 B), with a maximal rotation around the pore axis of ∼40° at aP309. This apparent rotation corresponds primarily to the lateral movement of each S6 helix and does not appear to involve substantial rotation within individual S6 helices themselves. Thus, there is a bulk counterclockwise movement of aSlo1 S6 around the pore axis (Fig. 4 B), whereas in the Kv1.2 morph, the most prominent changes in Cα positions begin to occur near the beginning of the PVP motif as the S6 helix moves outward from the pore axis (Fig. 4 B), perhaps reflecting internal helical rotation, occurring in concert with the outward movement of the S6 helix from the pore axis. We next measured the absolute distance of each S6 Cα carbon from the pore axis, for both aSlo1 structures (Fig. 4 C) and Kv1.2 structures (Fig. 4 D). In both cases, the orientation of homologous Cα-carbons around a given S6 helix and positions relative to the pore access are quite similar, as shown for the metal-free aSlo1 and the open Kv1.2 (Fig. 4 D). This seems surprising given that the pattern of MTS modification of introduced cysteines is quite different between BK and *Shaker*. One curiosity is that, although the distances of most Cα-carbons from the pore axis increase with opening in Kv1.2 (Fig. 4 E), this is not observed between the two aSlo1 structures (Fig. 4 E). For Slo1, it seems that the apparently nearer approach of some segment of S6 Cα carbons to the pore arises because of the bulk lateral motion of the Slo1 S6 helix, from being more at the corner of the "box," to more on the side. In contrast, for Kv1.2, the changes in Cα positions seem congruent with the widening of the Kv inner cavity. Nothing in the orientations of any of the known MTS-modifiable residues seems able to explain why some residues, but not others, are modified, or why there is any state dependence in modification rates.

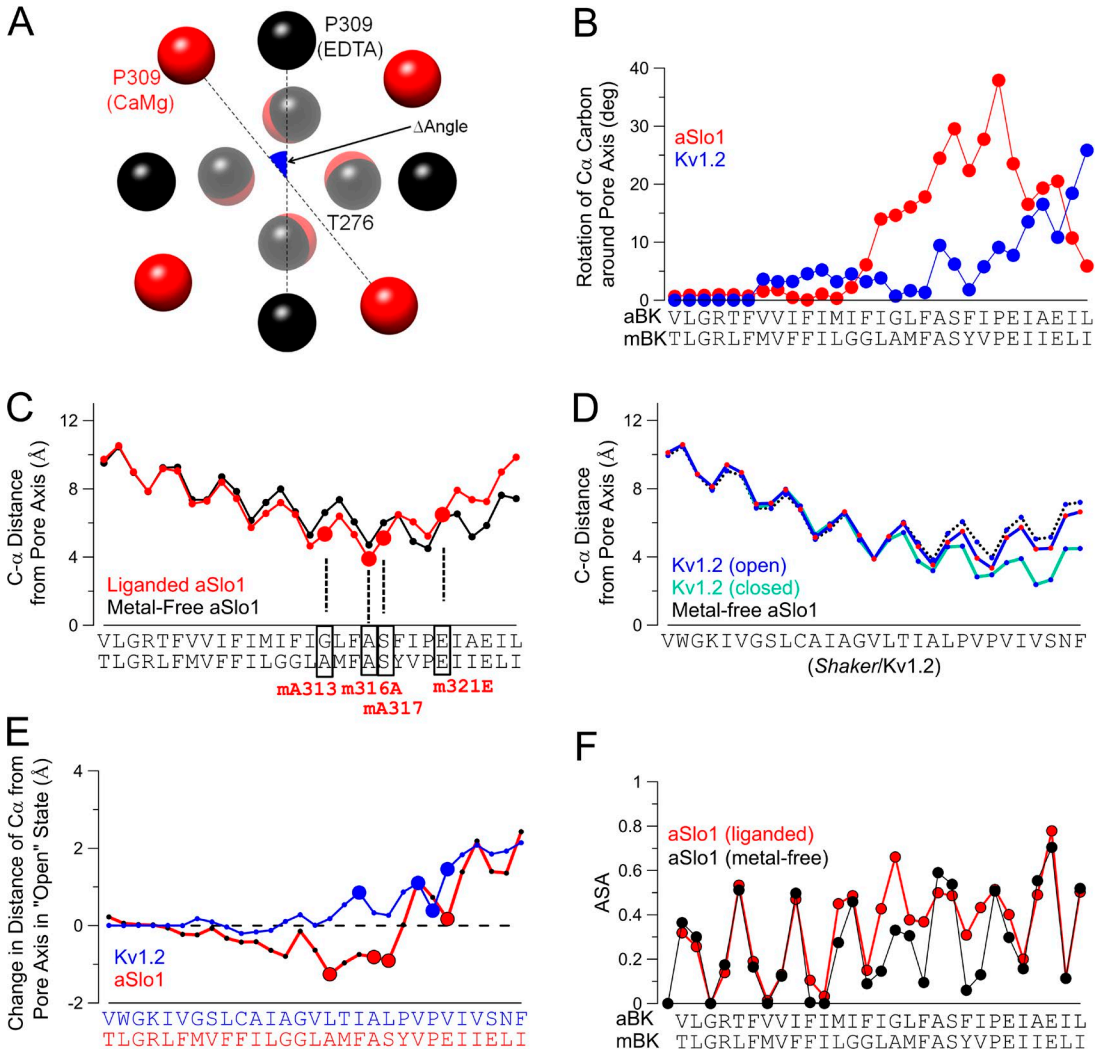


Figure 4. **Movement of S6 during gating.** Bulk motions of S6 appear to differ between Slo1 and Kv1.2, but changes in accessibility or orientation of aSlo1 S6 residues between liganded and metal-free structures are minimal. (A) Schematic showing counterclockwise movement of vector between diagonal Cα position of P309 residues between ligand-free (red) and liganded (blue) structures. ΔAngle corresponds to measured angle. (B) Plot of angular rotation determined as in A for aSlo1 (red) and Kv1.2 (black). (C) Comparison of absolute distance of Cα carbon from pore axis at each amino residue along S6 for liganded and metal-free Slo1 structures. Larger red circles correspond to residues readily modified by MTSET when substituted with Cys (mA313, mA316, mS317, mE321). (D) Similar comparison as in C, but for Kv1.2. Green line corresponds to metal-free Slo1 highlighting similarity in positioning of homologous residues between Kv1.2 and aSlo1 S6. (E) Change in Cα position relative to pore axis between more likely closed and open conformations for aSlo1 and Kv1.2. (F) Assessment of aqueous solvent accessibility for liganded and metal-free aSlo1 structures.

As a final comparison, we used a standard algorithm (Ahmad et al., 2004) for estimation of solvent accessibility of side chains (Fig. 4 F). Comparison between estimated solvent accessibility of side chains in the liganded aSlo1 versus metal-free aSlo1 reveals no consistent pattern of greater solvent accessibility of the known modifiable residues in the liganded conformation.

Despite the difference in bulk motions of the S6 α-helices, the general alignment of the aSlo1 Cα carbon positions with those in Kv1.2 relative to distance from the pore axis suggests there is no unusual feature of the S6 helix in aSlo1 that might distinguish it from other $K^+$ channels. However, compared with both Kv and mammalian Slo1 channels, the *Aplysia* S6 sequence is somewhat unusual. It is a rare $K^+$ channel lacking a glycine at the so-called hinge glycine position (Jiang et al., 2002b; Ding et al., 2005) and also lacks a pair of consecutive glycines found in mSlo1 at the hinge glycine position (see Fig. 2). *Aplysia* S6 contains a glycine at position 302, two residues after the canonical hinge glycine position, perhaps serving a similar functional role in permitting a bend in S6 during gating. Hite et al. (2017) noted two positions in S6 that contribute to bends in the helix that result in changes in shape and position of S6: aG302 (mA313) and aP309 (mP320). However, overall, these bends produce only modest differences in

the internal pore diameter between the two structures. Interestingly, from approximately aA305 to aP309, the metal-free Slo1 inner cavity appears to be wider than the liganded channel, although both aSlo1 inner cavities are wider than KvChim (Fig. 3 A). Near aE310, where the pore radius is ∼7–8 Å, the liganded aSlo1 inner cavity begins to widen relative to the metal-free inner cavity, eventually approaching a radius of ∼10 Å near aK317. The differences in positions of glycines between aSlo1 and mSlo1 in S6 raise the possibility that interesting differences between aSlo1 and mSlo1 may remain to be revealed.

On balance, then, there appears no aspect of the aSlo1 S6 structures that provides an explanation of the functional data related to gating shifts caused by charge substitutions or state-dependent modifications of introduced cysteines. Examination of S6 in the two aSlo1 structures does not reveal any obvious change in environment that might provide a structural basis for the idea that residues undergo state-dependent changes in accessibility or aqueous solubility that may favor a particular conformation. The absence of any indication of major bending or rotation between the aSlo1 S6 structures raises the question of how one is to explain the wealth of functional data suggesting that substantial conformational changes, perhaps involving helical rotation, occur in mammalian Slo1. As already noted, one possibility is that perhaps the S6 conformation in the metal-free structure represents an already significantly activated PGD. Another possibility may be that the structural changes associated with gating in aSlo1 are quite different from those in mSlo1, perhaps arising from such differences as positioning of glycine residues and the diglycine motif. Alternatively, mutations and other manipulations may alter structure and function in unanticipated ways. Clearly, such questions would benefit from structural information from a mammalian Slo1 PGD, functional data on aSlo1, or perhaps aSlo1 structures with mutated S6 residues.

### Sensor domains in Slo1

In this section, we examine the topics of ligand and voltage sensing and how the CTD and VSD sensor domains couple to channel activation, within the context of whether structure-function studies are fully congruent with newly available structural information.

**$Ca^{2+}$-binding sites and $Ca^{2+}$-induced conformational changes.** Functional studies have defined two distinct high-affinity $Ca^{2+}$-binding sites in the CTD of each Slo1 α subunit for a total of eight binding sites per channel. The first putative $Ca^{2+}$-binding site was identified from mutations of a cluster of acidic residues, now dubbed the $Ca^{2+}$ bowl, that reduce $Ca^{2+}$-dependent activation (Schreiber and Salkoff, 1997). This study together with other mutational analysis showed that side chains of residues mD898 (aD905) and mD900 (aD907) are essential for $Ca^{2+}$ coordination (Bao et al., 2004). Typically, $Ca^{2+}$-dependent activation is quantified as the $Ca^{2+}$-dependent shift in the G-V relationship to more negative voltages. Mutations of the $Ca^{2+}$ bowl reduced $Ca^{2+}$-dependent activation such that the shift of the G-V relation in response to saturating $Ca^{2+}$ concentrations is just more than half of that in the WT channels (Schreiber et al., 1999; Bian et al., 2001). This residual $Ca^{2+}$-dependent activation suggested that additional $Ca^{2+}$ activation sites might remain to be identified.

Progress on $Ca^{2+}$-dependent regulation of Slo1 channels and identification of a second putative $Ca^{2+}$-binding site were greatly aided by the crystal structure of the RCK domain of the *E. coli* $K^+$ channel (Jiang et al., 2001). Remarkably, this domain exhibited strong homology to two separate segments, now termed RCK1 and RCK2, within the extensive cytosolic sequence of mammalian Slo1. Guided by the position of nucleotide-binding residues in the *E. coli* RCK domain, mutational analysis of acidic residues within RCK1 revealed a second area of the Slo1 cytosolic domain that influenced $Ca^{2+}$ sensitivity (Shi et al., 2002; Xia et al., 2002; Zhang et al., 2010). Mutations of these residues abolished an additional component of $Ca^{2+}$-dependent activation (Shi et al., 2002; Xia et al., 2002; Sweet and Cox, 2008; Zhang et al., 2010) such that combined mutation of $Ca^{2+}$ bowl residues and the mD367 residue in RCK1 removed all activation by $Ca^{2+}$ at concentrations up to ∼1 mM. That regulation by $Ca^{2+}$ reflects two distinct $Ca^{2+}$ coordination sites located in the CTD has also been supported by work showing that the two sites have distinct divalent cation selectivity (Schreiber and Salkoff, 1997; Zeng et al., 2005; Zhou et al., 2012). The possibility that some $Ca^{2+}$ regulation might arise from sites other than the CTD has been excluded by demonstration that replacement of the mouse Slo1 CTD with the CTD of the pH-regulated mouse Slo3 channel abolished all regulation by $Ca^{2+}$ (Xia et al., 2004) and, additionally, removing the CTD removes all $Ca^{2+}$ and $Mg^{2+}$ sensitivity (Budelli et al., 2013).

Subsequently, the crystal structures of MthK (Jiang et al., 2002a,b), containing a PGD and a large CTD comprising eight identical RCK domains, provided a powerful template for generation of useful homology models of the Slo1 channel gating ring (Jiang et al., 2002a). The homology models allowed better placement of the two $Ca^{2+}$ sites within the overall Slo1 gating ring, with the $Ca^{2+}$ bowl located in RCK2 and the mD367 site within the more N-terminal part of RCK1. This also led to identification of E535 as another potential $Ca^{2+}$-coordinating residue in the C-terminal lobe of RCK1 (Zhang et al., 2010). The close positioning of mD367 and mE535 in RCK1 was later supported by the isolated hSlo1 gating ring structure (Wu et al., 2010). Molecular dynamic simulations based on this structure suggested that the

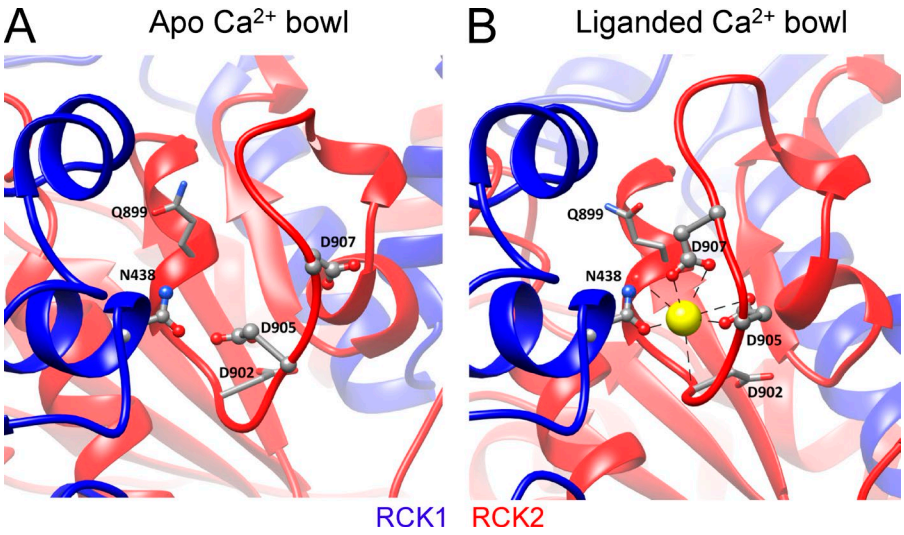


Figure 5. **The $Ca^{2+}$ bowl.** (A) High-resolution view of the metal-free aSlo1 structure from a portion of the RCK2 domain containing the $Ca^{2+}$ bowl. $Ca^{2+}$ coordinating residues are labeled (*Aplysia* numbering). Structures in A and B were aligned based on the αD helix in RCK1, which contains residue aN438 (mN449), proposed to provide a basis for cooperativity between $Ca^{2+}$ binding in RCK1 and RCK2 of adjacent subunits. (B) View of the liganded aSlo1 structure showing $Ca^{2+}$ coordination in the $Ca^{2+}$ bowl. Residues that coordinate via backbone carbonyl are shown with stick side chains.

side chain of mD367 (aD356), mE535 (aE525), and also the backbone carbonyl of mR514 (aR503) contribute to $Ca^{2+}$ coordination in RCK1 (Zhang et al., 2010).

Consistent with functional inferences, the liganded aSlo1 structure now reveals density corresponding to $Ca^{2+}$ ion in both $Ca^{2+}$-binding sites (Tao et al., 2017). The liganded structure confirms some $Ca^{2+}$-coordinating residues and also identifies new ones. For $Ca^{2+}$ coordination in the $Ca^{2+}$ bowl site (Fig. 5, A and B), both isolated Slo1 CTD structures (Yuan et al., 2010, 2011) and the liganded aSlo1 structure show that in addition to the side chains of the two functionally identified residues mD898 (aD905) and mD900 (aD907; Bao et al., 2004), the carbonyl oxygen atoms from the backbone of mQ892 (aQ899) and mD895 (aD902) also contribute to $Ca^{2+}$-binding in the $Ca^{2+}$ bowl (Yuan et al., 2010; Tao et al., 2017). Interestingly, the side chain carboxamide of an asparagine (mN449/aN438) in the RCK1 domain from an adjacent subunit is found to directly contact with the $Ca^{2+}$ bound in the $Ca^{2+}$ bowl, indicating that the $Ca^{2+}$ bowl site may be influenced by $Ca^{2+}$ occupancy status of RCK1 in a neighboring subunit. This provides a potential structural basis for functional interactions between the two $Ca^{2+}$-binding sites. For the RCK1 site (Fig. 6, A and B), the structure confirms the role of mD367 (aD356) and mE535 (aE525) side chains and mR514 (aR503) main chain carbonyl in $Ca^{2+}$ coordination, while also identifying other $Ca^{2+}$ coordinating residues in the RCK1 site, including mS534 (aG523) and mS602 (aE591), that bind to $Ca^{2+}$ with their backbone carbonyls. Except for mD367 (aD356) in the N-terminal lobe, all other $Ca^{2+}$ coordinating residues are located at the C-terminal lobe of RCK1.

**Potential interactions of the CTD with the PGD.** An important question concerning Slo1 channel function is

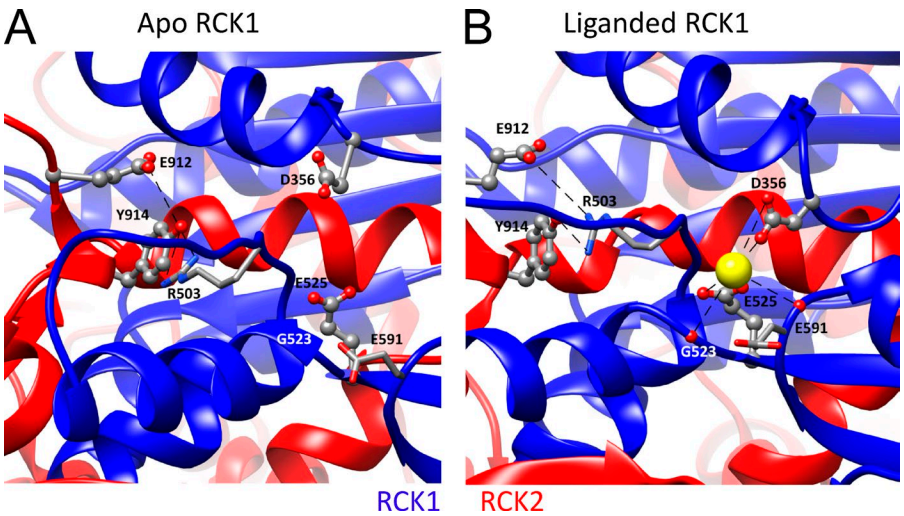


Figure 6. **The RCK1 $Ca^{2+}$-binding sites.** (A) High-resolution view of the metal-free structure surrounding the RCK1 $Ca^{2+}$-binding sites with coordinating residues labeled. Structures in A and B were aligned by the RCK2 αS helix that resides in the vicinity of the RCK1 binding site, but appears to undergo no major change between structures. (B) High-resolution view of the liganded aSlo1 structure surrounding the RCK1 binding site with coordination mediated by backbone carbonyls of aR503 (mR514), aG523 (mS533), and aE591 (mS600) and side chains of aD356 (mD367) and aE525 (mE535). Electrostatic interaction between aE912/aY914 near the $Ca^{2+}$ bowl of the same subunit with the side chain of aR503 is proposed to underlie potential interactions between RCK1 and $Ca^{2+}$ bowl binding sites.

how $Ca^{2+}$-binding in the CTD is transduced into an effect on PGD opening. The CTD of Slo1 and the pore-lining S6 in the PGD are covalently connected by a peptide linker of 15 amino acids known as the C-linker. Based on the MthK structure, this linker was naturally proposed to transmit $Ca^{2+}$-induced conformational changes in CTD to the PGD of Slo1 (Jiang et al., 2002a,b). However, for some bacterial RCK-containing proteins, the cytosolic module containing the RCK domains is not directly covalently tethered to the pore domain (Lingle, 2007; Cao et al., 2013), suggesting that RCK domains can regulate channel/transporter fashion by mechanisms unrelated to any C-linker connection.

For Slo1, the potential role of the C-linker was addressed by examination of gating with amino acids inserted in or removed from the C-linker. Voltage- and $Ca^{2+}$-dependent activation of Slo1 was negatively correlated with the C-linker length (Niu et al., 2004). This led to the proposal that the C-linker, the gating ring, or both acting in series act like a passive spring such that $Ca^{2+}$ binding directly pulls the C-linker to open the gate. The functional data were not sufficient to distinguish whether the spring arises from the C-linkers, the gating ring, or both (Niu et al., 2004). The structural data may provide new information on this question. in both the liganded and metal-free structures, the C-linkers adopt essentially identical conformations of the same length, but that the N-terminal lobe of the gating ring moves considerably (Hite et al., 2017). This result suggests that, at least between these two structures, the C-linker alone does not act like a spring in influencing pore conformation (Hite et al., 2017), leaving open the possibility that the N-lobe of the gating ring may contribute spring-like properties.

The elements of the CTD that might be involved in transducing $Ca^{2+}$ signals were further addressed by a comparison of $Ca^{2+}$-dependent activation between mSlo1 and *Drosophila* Slo1 (dSlo1; Krishnamoorthy et al., 2005). This work identified an amino acid sequence in the N-terminal lobe of RCK1 responsible for a greater $Ca^{2+}$-dependent activation in dSlo1 than in mSlo1. Subsequently, it was found that the N-terminal lobe of RCK1 makes direct contact with the membrane-spanning VSD, contributing to a $Mg^{2+}$-binding site (see section $Mg^{2+}$-dependent gating) and direct noncovalent interactions between the two domains (Yang et al., 2008, 2013). Based on homology modeling, the N-terminal lobe of RCK1 was shown to be the only part of the entire CTD that may make contacts with the membrane-spanning domain (Lee et al., 2010), suggesting that any conformational changes in the CTD upon $Ca^{2+}$ binding may propagate via the N-terminal lobe of RCK1 to the PGD to open the channel. Thus, functional studies have suggested that gating ring status can influence the PGD through two distinct physical linkages: one, the direct CTD-PGD connection through the C-linker, and the other, an indirect connection between the CTD with the VSD/PGD through noncovalent interactions (Lee et al., 2010; Yang et al., 2015; Yang and Cui, 2015).

This idea is consistent with the aSlo1 structures, which show the N-lobe of RCK1 in close contact with the VSD and the S4–S5 linker, forming a specific protein–protein interface (585 $Å^2$ per subunit in the liganded structure; Hite et al., 2017; Tao et al., 2017). This protein–protein interface changes between the liganded and the metal-free structures, suggesting that noncovalent interactions, in addition to any role of the C-linker, may also be important for connecting $Ca^{2+}$ binding to pore opening (Hite et al., 2017).

**Are there interactions between the two $Ca^{2+}$-binding sites?** The presence of two distinct kinds of $Ca^{2+}$-binding sites in each Slo1 subunit has naturally raised the question about the interaction and relationship between the two sites in producing channel activation. As an allosteric protein with multiple $Ca^{2+}$-binding sites that are spatially separated, activation is favored by increased $Ca^{2+}$ occupancy of available sites, and it is the higher-affinity binding of $Ca^{2+}$ to open channels that drives activation (McManus and Magleby, 1991; Cox et al., 1997; Horrigan and Aldrich, 2002). In this case, the determinants of higher affinity in the open state might be considered the basis for cooperativity. However, it could be imagined that occupancy of one kind of $Ca^{2+}$-binding site might alter the intrinsic affinity of the second kind of $Ca^{2+}$-binding site in either the closed or open state. The currently available functional and structural data are insufficient to address such nuances, and here we only consider the functional and structural features that address whether there may be interactions between sites.

In early work, the $Ca^{2+}$-dependent G-V shifts in WT channels were shown to be approximately identical to the sum of the gating shifts produced by an intact $Ca^{2+}$ bowl or an intact RCK1 domain each acting alone (Xia et al., 2002). This result suggested that the two $Ca^{2+}$ sites acted largely independently in activating the channel. However, more precise measurements of $Ca^{2+}$-dependent changes in open probability (Po) showed that the sum of increases in Po by $Ca^{2+}$ binding to each of the two $Ca^{2+}$ sites is larger than the total $Ca^{2+}$-dependent Po increases of the WT Slo1 channel (Sweet and Cox, 2008), suggesting a negative cooperativity with a cooperativity factor of 0.75 between the two $Ca^{2+}$ sites. Voltage clamp fluorimetry measurements with fast $Ca^{2+}$ application via UV photolysis of caged $Ca^{2+}$ have also reported a negative cooperativity between the RCK1 site and the $Ca^{2+}$ bowl (Savalli et al., 2012). However, another elegant study, using measurements of single-channel Po for channels of defined $Ca^{2+}$-binding site stoichiometry, showed that $Ca^{2+}$ is more effective in activating Slo1 channels with both $Ca^{2+}$-binding sites

active in the same subunit than in those with the two active sites in different subunits. This result supports positive cooperativity between RCK1 and $Ca^{2+}$ bowl sites within the same subunit, whereas channels with active RCK1 sites alone, active $Ca^{2+}$ bowl sites alone, or active RCK and $Ca^{2+}$ bowl sites on different subunits behave as if all sites were independent (Qian et al., 2006). The basis of the differences between the results of Sweet and Cox (2008) and those from Qian et al. (2006) is uncertain and could be impacted by analytical and methodological differences. However, overall, the extent of cooperativity, either negative or positive, in both studies may be considered rather modest.

Despite these uncertainties about the extent and nature of any cooperativity in Slo1 activation, the liganded aSlo1 structure suggests some provocative new features that may be related to interactions between binding sites. First, despite the $Ca^{2+}$ bowl being largely determined by residues within RCK2, $Ca^{2+}$ coordination not only is defined by the loop of acidic residues, but also is influenced by aN438 (mN449; Fig. 5 B) from RCK1 of the adjacent subunit (Yuan et al., 2010; Tao et al., 2017). For the RCK1 site, most coordinating residues are located in the C-lobe, whereas only mD367 resides in the N-lobe (Fig. 6 B). Thus, both sites use coordination from residues contributed from distinct lobes or domains of the CTD. Hite et al. (2017) propose that the completion of $Ca^{2+}$ binding in both sites pulls two subdomains involved in each site together and supports a rigid body movement of the N-terminal lobe of RCK1 to open the channel. Based on the idea that movement of the N-terminal lobe of RCK1 may be required to complete $Ca^{2+}$ binding in both sites, the binding in the two sites is proposed to be positively cooperative via this movement (Hite et al., 2017). However, mutational analysis does not as yet support some aspects of this proposal. Although aN438 located in RCK1 is proposed to contribute to $Ca^{2+}$ coordination in the $Ca^{2+}$ bowl, the functional role of this residue in $Ca^{2+}$-dependent activation in mSlo1 (mN449) has not been fully evaluated. Second, the liganded aSlo1 structure also suggests that the two $Ca^{2+}$-binding sites within a single Slo1 subunit may be interconnected by an electrostatic interaction between the aR503 in the RCK1 site and aE912/aY914 in the loop after the $Ca^{2+}$ bowl (Fig. 6; Tao et al., 2017). Such an interaction might also underlie changes in agonist affinity associated with channel or gating ring activation. Overall, the structural studies provide support for the idea that $Ca^{2+}$-binding sites both on the same subunits and between subunits may interact. To what extent either of the observed interactions between binding sites may underlie the available functional results is unclear. One testable idea would be to determine whether the previously reported intra-subunit positive cooperativity (Qian et al., 2006) is abolished with disruption of the intra-subunit electrostatic interaction. Given the small and conflicting nature of the results addressing cooperativity between the two kinds of $Ca^{2+}$-binding sites, the issue is likely to be challenging to address.

Does each kind of $Ca^{2+}$-binding site act to produce the same overall conformational change in the gating ring that then opens the PGD, or are there functional and structural differences in how each binding site may influence gating (Hite et al., 2017)? In essence, this is the question of how ligand binding couples to channel opening. A standard approach to this question is to try to identify amino acids that, when mutated, interfere with channel opening, although not in any way affecting $Ca^{2+}$ binding per se. Several residues in the N-lobe of RCK1 have been proposed to meet these criteria (Yang et al., 2010), i.e., they are not thought to influence $Ca^{2+}$ coordinating residues, but disrupt $Ca^{2+}$-dependent activation mediated by the RCK1 domain. Mutation of these N-lobe residues fails to inhibit the $Ca^{2+}$ bowl–dependent activation when only the RCK1 $Ca^{2+}$ site is destroyed by the mD367A mutation, but substantially reduces RCK1 dependent activation when the $Ca^{2+}$ bowl site is rendered inoperable by the 5D5N mutations. Under the assumption that these mutations do not alter the affinity of $Ca^{2+}$ for the RCK1 site, it has been suggested that the N-lobe of RCK1 is involved in the ability of RCK1 $Ca^{2+}$ binding to act on the PGD domain but does not participate in activation involving the $Ca^{2+}$ bowl (Yang et al., 2010). Irrespective of whether these RCK1 N-lobe residues are directly involved in coupling, the results support a clear distinction between the RCK1 and RCK2 domains in how they contribute to channel opening. Another residue known to interfere with $Ca^{2+}$-dependent activation mediated by the RCK1 $Ca^{2+}$ site, but not the $Ca^{2+}$ bowl site, is mM513 (Bao et al., 2002). These results have been taken to indicate that the machinery of channel activation resulting from $Ca^{2+}$ binding to the RCK1 site is different from that resulting from binding at the $Ca^{2+}$ bowl. Two other results also support this. First, activation involving the RCK1 site was shown to be sensitive to voltage, whereas activation involving the $Ca^{2+}$ bowl is not (Sweet and Cox, 2008). Second, voltage clamp fluorimetry measurements suggest that $Ca^{2+}$ binding to the RCK1 and $Ca^{2+}$ bowl sites affect voltage sensor activation differently (Savalli et al., 2012). Overall, these results suggest that the pathway through which $Ca^{2+}$ binding in RCK1 leads to channel activation differs from that involving $Ca^{2+}$ binding in the $Ca^{2+}$ bowl (Yang et al., 2010; Yang and Cui, 2015).

### $Mg^{2+}$-dependent gating

Slo1 channels are regulated not only by cytosolic $Ca^{2+}$, but also millimolar $Mg^{2+}$. The new structures provide detailed pictures of the determinants of $Mg^{2+}$ coordination, supporting many aspects of earlier biophysical inferences.

**Slo1 contains a low-affinity $Mg^{2+}$-binding site.** In addition to $Ca^{2+}$, millimolar intracellular $Mg^{2+}$ can activate

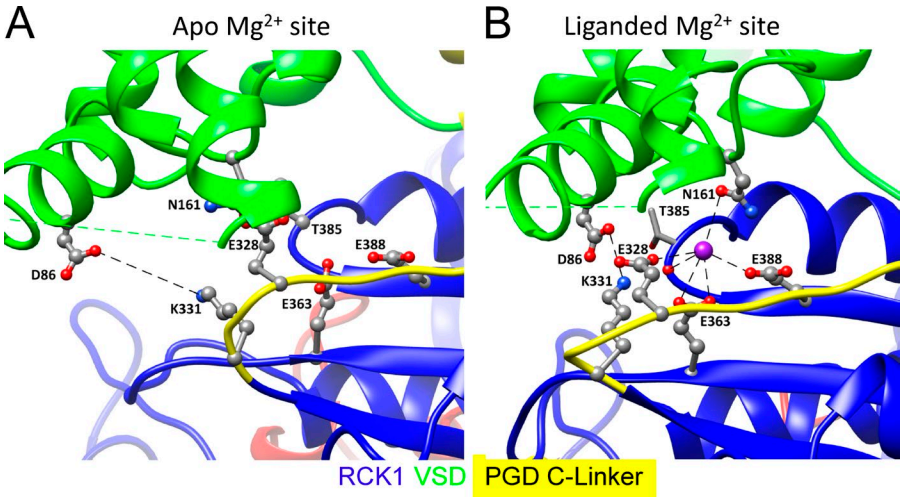


Figure 7. **The $Mg^{2+}$-binding site.** (A) High-resolution view of the metal-free structure in the vicinity of the $Mg^{2+}$-binding site. Alignment was based on the S0′ segment (Tao et al., 2017) which is part of the linker between the S0 and S1 TM segments. (B) In the $Mg^{2+}$ liganded structure, side chains of aN161 (mN172), aE328 (mV339), aE363 (mE374), and aE388 (mE399), along with the backbone carbonyl of T385 (mT396), appear to contribute to $Mg^{2+}$ coordination, whereas residues aD86 (mD99) and aK331 (mR342) form a salt bridge that may help stabilize the bound $Mg^{2+}$ structure. Dotted green lines reflect cytosolic loops not defined in the structure.

Slo1 channels (Golowasch et al., 1986; Oberhauser et al., 1988). In fact, $Mg^{2+}$-dependent activation occurs independently of activation produced by micromolar $Ca^{2+}$, as indicated by the almost identical shifts of the $Mg^{2+}$-induced activation curves in the presence and absence of saturating [$Ca^{2+}$] (Shi and Cui, 2001; Zhang et al., 2001), indicative that activation by millimolar $Mg^{2+}$ occurs by a distinct mechanism. Consistent with this, mutagenesis identified that mE374 and mE399 (aE363 and aE388) in the N-lobe of RCK1 are critical for $Mg^{2+}$ but not $Ca^{2+}$ sensing (Shi et al., 2002; Xia et al., 2002). Subsequent work identified two more oxygen-containing residues in the VSD that can serve as additional putative $Mg^{2+}$ binding residues: mD99 (aD86) in the C terminus of the long S0–S1 loop and mN172 (aN161) in the S2–S3 loop (Yang et al., 2008). Consistent with their roles in $Mg^{2+}$ coordination, the side chain properties of mD99 and mN172 are critical for $Mg^{2+}$ sensitivity. In addition, disulfide cross-linking suggests that the $Mg^{2+}$ binding residues from the VSD and the CTD are spatially close to each other (Yang et al., 2008). Thus, $Mg^{2+}$ binds to an interdomain binding site that is composed of residues from both the VSD and the CTD (Fig. 7, A and B).

That the $Mg^{2+}$-binding site is formed between two distinct domains, the VSD and CTD, raised a question about the spatial arrangement of the $Mg^{2+}$ binding residues in the quaternary structure. Are the residues coordinating $Mg^{2+}$ between the two domains from the same subunit or different subunits? To answer this, heterotetrameric mSlo1 channels formed by mixing the single mutations of D99R or N172R from the VSD and E374R or E399C from the CTD were shown to exhibit significant $Mg^{2+}$ sensitivity, whereas heterotetrameric channels resulting from the mixture of D99R and N172R in the VSD or from the mixture of E374R and E399C in the CTD completely lost their $Mg^{2+}$ sensitivity (Yang et al., 2008). These results seemed paradoxical because individual mutation of any of these four $Mg^{2+}$ binding residues can completely abolish $Mg^{2+}$ sensitivity in homotetrameric Slo1 channels. Thus, formation of an inter-subunit $Mg^{2+}$-binding site, where the $Mg^{2+}$ binding residues in the VSD and the CTD derive from two neighboring subunits, provides the only plausible explanation. These results suggest that the VSD of one subunit aligns with the CTD of a neighboring subunit to form the $Mg^{2+}$-binding site (Yang et al., 2008; Yang and Cui, 2015). This finding thus predicted an unusual quaternary structural arrangement of the VSD relative to the CTD, which is now perfectly explained by the non–domain-swapped VSD arrangement in the aSlo1 structure (Tao et al., 2017).

Overall, there is a satisfying concordance between functional and structural evidence regarding the determinants of $Mg^{2+}$ coordination. Specifically, in the liganded aSlo1 structure (Tao et al., 2017), the side chains of aN161 (mN172), aE363 (mE374), and aE388 (mE399) directly coordinate a $Mg^{2+}$ ion (Fig. 7, A and B), consistent with previous functional findings (Shi et al., 2002; Xia et al., 2002; Yang et al., 2008). These three residues provide four oxygen coordinates for $Mg^{2+}$, in which aN161 and aE388 are monodentate and aE363 is bidentate (Tao et al., 2017). The aSlo1 structure also reveals some features that were not observed in previous functional characterizations. First, the main-chain carbonyl oxygen atom of aT385 (mT396) and a water molecule were assigned to provide another two $Mg^{2+}$ coordinates (Tao et al., 2017). Second, an oxygen atom from the side chain of aE328 (mV339 in mSlo1), an acidic residue in the C-linker region, is spatially close to the bound $Mg^{2+}$ ion (3.8 Å apart) in the aSlo1 structure. Although this residue was not emphasized in the original paper (Tao et al., 2017), its side chain oxygen is highly likely to provide one additional $Mg^{2+}$ coordinate. This would bring the total number of $Mg^{2+}$ coordinates to seven, which is inconsistent with the octahedral coordination chemistry of $Mg^{2+}$ that requires six oxygen coordinates. Unfortunately, no functional evidence from

mammalian Slo1 channels can help solve this paradox because the corresponding residue of aE328 in mSlo1 is a valine (mV339), which does not contain oxygen in its side chain. Third, even though the side chain of aD86 (mD99 in mSlo1) in the aSlo1 structure stays in the vicinity of $Mg^{2+}$ ion and other $Mg^{2+}$ coordinates (Yang et al., 2008; Tao et al., 2017), this residue seems unlikely to coordinate $Mg^{2+}$ in aSlo1 because the distance between its side chain oxygen and $Mg^{2+}$ is too great (5.8 Å). Instead, aD86 is proposed to play an important role in stabilizing the $Mg^{2+}$ binding site (Tao et al., 2017) by interacting with some other nearby charged residues, including aK331 (mR342). Whether interaction between aD86 and aK331 (mD99 and mR342) underlies the fact that mutation of mD99A completely abolishes $Mg^{2+}$ sensitivity (Yang et al., 2008) will require further study. Overall, despite some discrepancies, the structural and functional results regarding determinants of $Mg^{2+}$ binding are in good agreement.

Conformational changes associated with $Mg^{2+}$-dependent gating. Electrophysiological experiments suggest that $Mg^{2+}$ activates BK channels through an electrostatic interaction with the gating charge residue mR213 (aR202) in the S4 of the VSD (Hu et al., 2003; Yang et al., 2007). 10 mM $Mg^{2+}$, as well as a positive charge on residue 397 (mQ397R) that is in the vicinity of the $Mg^{2+}$-binding site, can activate mSlo1 channels by directly affecting the VSD movement from its activated state to the resting state. Because VSD movement from the active state to resting state is slowed, this is seen as a smaller and slower OFF gating current (Yang et al., 2007; Horrigan and Ma, 2008). Neutralization of R213 specifically abolishes the activation effect of millimolar $Mg^{2+}$ and Q397R, further supporting that this interaction is electrostatic by nature (Hu et al., 2003). No mutations of other charged residues in the VSD abolish $Mg^{2+}$ sensitivity, although E219R reduces $Mg^{2+}$ sensitivity slightly (Hu et al., 2003; Yang et al., 2007). Based on an electrostatic interaction model, the estimated distance between R213 and Q397R when the VSD is in the resting state is approximately 9 Å (Yang et al., 2007).

The measurements of $Mg^{2+}$ effects on gating currents show a state-dependent interaction between the bound $Mg^{2+}$ and the VSD. The effect of $Mg^{2+}$ on the OFF gating current, a measure of VSD returning from activated state to resting state, is much stronger when the channel is open: with the increase in the fraction of open channels during the rising phase of current activation, the reduction of the OFF gating current is increased. $Mg^{2+}$ does not alter VSD activation when the channel is closed, which is further indicated by the minimal effect of $Mg^{2+}$ on the ON gating current (Yang et al., 2007, 2008; Horrigan and Ma, 2008; Chen et al., 2011). Subsequently, single-channel data suggested that $Mg^{2+}$ could bind in both open and closed BK channels but only activates the channel when the VSD is in the activated state (Chen et al., 2011). These results led to the proposal of a structural rearrangement around the $Mg^{2+}$-binding site upon channel opening, such that the distance between R213 and the bound $Mg^{2+}$ becomes larger with channel closing.

At present, the structural data are insufficient to fully evaluate the structural basis of the $Mg^{2+}$ regulatory effects. In both metal-free and liganded aSlo1 structures, the distance between aQ386 (mQ397), a residue thought to participate in $Mg^{2+}$ binding in mSlo1, and aR202 (mR213), a S4 gating charge residue thought to make electrostatic interactions with the bound $Mg^{2+}$ in mSlo1, is ∼22–23 Å, much larger than the ∼9 Å predicted in the resting state functional studies in mSlo1 (Hu et al., 2003; Yang et al., 2007, 2008). Functional studies propose a state-dependent interaction between $Mg^{2+}$ and mR213, and the distance between aQ386 and aR202 would potentially be consistent with the proposed weak electrostatic interaction between bound $Mg^{2+}$ and the VSD in the liganded state (Horrigan and Ma, 2008). However, neither structure (Tao et al., 2017) provides actual support for an interaction between $Mg^{2+}$ and aR202 (mR213). Thus, whether $Mg^{2+}$ might act on the aSlo1 VSD remains unclear.

Additional functional and structural data on aSlo1 and structural data on full-length mSlo1 might help address these issues. Of particular value would be liganded Slo1 structures with mutated $Mg^{2+}$-coordinating residues, e.g., aE363A and aE388A, or $Mg^{2+}$-ligated structures, with both $Ca^{2+}$ sites mutated.

## Voltage-dependent activation

Activation of Slo1 channels by voltage exhibits several features distinct from that noted for Kv channels (Ma et al., 2008). Although the new structures do not explicitly compare effects of voltage on Slo1 structure, differences in VSD structure and interactions of the VSD with other domains provide potential insight into the role of Slo1 VSDs in BK gating.

The Slo1 voltage-sensor and voltage-dependent activation of Slo1. Like Kv channels, Slo1 channels contain a discrete voltage-sensor domain formed by S1–S4 membrane-spanning segments. Both Kv and Slo1 share some conserved structural features such as an extracellular $Cu^{2+}$-binding site, which in the Slo1 VSD involves four residues from S1, S2, and S4 transmembrane segments (Ma et al., 2008). However, the overall magnitude of the charge moved and kinetic aspects of the movement differ markedly between Slo1 and Kv. Voltage dependence of Slo1 gating has been examined by direct measurements of gating charge movements (Stefani et al., 1997; Horrigan and Aldrich, 1999), voltage-dependent activation in the absence of $Ca^{2+}$ binding (Cox et al., 1997; Cui et al., 1997; Stefani et al., 1997; Díaz et al.,

1998; Rothberg and Magleby, 2000; Ma et al., 2006), and recently, voltage-dependent activation of a truncated mSlo1 channel containing only the PGD and VSD, with the entire cytosolic domain after the C-linker removed (Budelli et al., 2013; Zhang et al., 2017). Similar to Kv channels, the Slo1 S4 contains regularly spaced basic residues, mR207, mR210, and mR213, that correspond to the canonical voltage-sensing R2, R3, and R4 residues in Kv S4. However, unlike Kv channels, mutations that neutralize charged residues suggest that only mR213, but not mR207 or mR210, contributes to measured gating charge. Instead, charged residues mD153 and mR167 in S2 and mD186 in S3 also contribute to gating charges (Ma et al., 2006) and perhaps mE219 in S4 (Zhang et al., 2014). Overall, Slo1 channels exhibit a relatively weak voltage dependence compared with Kv channels, with a total gating charge valence of 2.32e (Horrigan and Aldrich, 1999; Rothberg and Magleby, 2000; Chen et al., 2011; Zhang et al., 2014), and each of the above charged residues in each of the four mSlo1 subunits accounts for less than 0.3e gating charge (Ma et al., 2006). These results led to the suggestion that, unlike a large S4 movement during voltage sensing in Kv channels, the VSD of Slo1 may undergo small movements of S2, S3, and S4 in response to changes in voltage (Ma et al., 2006). This proposed modest S4 movement is also supported by measurements of MTS reagent accessibility of S4 charged residues (Hu et al., 2003) and fluorescence measurements of the movements of S2 and S4 segments (Pantazis et al., 2010) during voltage-dependent gating.

Some structural features of the aSlo1 VSD differ from the Kv VSD. The Slo1 VSD exhibits both similarities and differences from Kv VSDs. As with Kv, the S1–S4 helices of aSlo1 structures are arranged compactly, consistent with a role as a modular voltage-sensing apparatus (Tao et al., 2017). Mammalian Slo1 proteins also contain an additional S0 transmembrane segment (Meera et al., 1997), which has been implicated as part of the VSD apparatus. In particular, mutations in the extracellular part of mammalian S0 have substantial effects on voltage-dependent gating (Koval et al., 2007), whereas disulfide crossing linking experiments indicate that the extracellular end of S0 closely interacts with the extracellular end of S3 and S4 (Liu et al., 2008), consistent with a role of S0 as an integral part of the VSD. Generally consistent with this, the extracellular ends of S0, S3 and S4 are positioned close together in the aSlo1 structures. However, much of the length of S0 does not seem to assemble as an integral part of the VSD in aSlo1 (Tao et al., 2017). Given the large number of residues that are entirely unique to aSlo1 S0 compared with mSlo1 S0, it is possible that the functional role of S0 in aSlo1 may differ somewhat in comparison to mammalian Slo1.

Another unexpected aspect of the aSlo1 VSD is that, whereas in Kv channels the VSD resides just outside the S5-P loop-S6 of an adjacent subunit (Long et al., 2005a, 2007), in Slo1 channels, the VSD is adjacent to the pore of the same subunit. In the aSlo1 structures, S4 in the VSD is packed tightly in an antiparallel fashion with S5 in the pore gate domain, perhaps restricting the movement of S4 (Tao et al., 2017). In addition, the S3–S4 paddle and charge transfer center that are important for gating charge movements in other Kv channels do not exist in aSlo1 (Tao et al., 2017). These structural features may explain the functional observations that gating charge arises from a decentralized distribution of voltage-sensing residues and that charged residues in S2, S3, and S4 make only small contributions to gating charge in Slo1 channels (Ma et al., 2006). That each VSD of aSlo1 closely abuts the PGD of the same subunit, whereas, in Kv channels, each VSD abuts an adjacent subunit, may contribute to differences in how the VSD in each type of channel couples to the PGD and, ultimately, channel activation.

Differences in the Slo1 VSD between metal-free and liganded structures. Although both aSlo1 structures were obtained at nominal 0 mV, there are differences in the VSDs between the structures (Fig. 8, A and B). The cytosolic ends of various TM segments relative to the pore axis undergo changes (Fig. 8 A), e.g., the S4 cytosolic end moves outward from the pore axis in the liganded structure. Furthermore, there is a small displacement of mR213 (aR202) toward the extracellular side in the aSlo1 VSD in the liganded channel (Fig. 8, B and C). However, these changes are quite small compared with S4 movements thought to occur in Kv channels in response to voltage changes. Whereas the vertical movement of the R4 side chain (R303 in Kv1.2) in the VSD of Kv channels is estimated to be more than 16 Å in response to depolarization (Pathak et al., 2007), the vertical movement of the aR202 side chain (mR213, homologous to Kv R4) between the two aSlo1 structures is less than 5 Å (Fig. 8 C). Another difference between the aSlo1 VSD and that proposed for Kv1.2 (Pathak et al., 2007) in closed channels is that the aSlo1 R4 residue in the VSD is already partially displaced toward the extracellular side of the membrane, relative to the R4 position in Kv1.2. Together, both the position of Slo1 mR213 (a203) and its rather modest movement seem generally consistent with the earlier proposal based on functional tests that the resting VSD position is already partially activated relative to Kv channels (Ma et al., 2006). However, whether the observed change in VSD position in aSlo1 is quantitatively consistent with measured gating charge is not clear.

Several factors suggest that inferences about changes in the aSlo1 VSD position should probably be taken with some caution. First, voltage by itself is ostensibly not

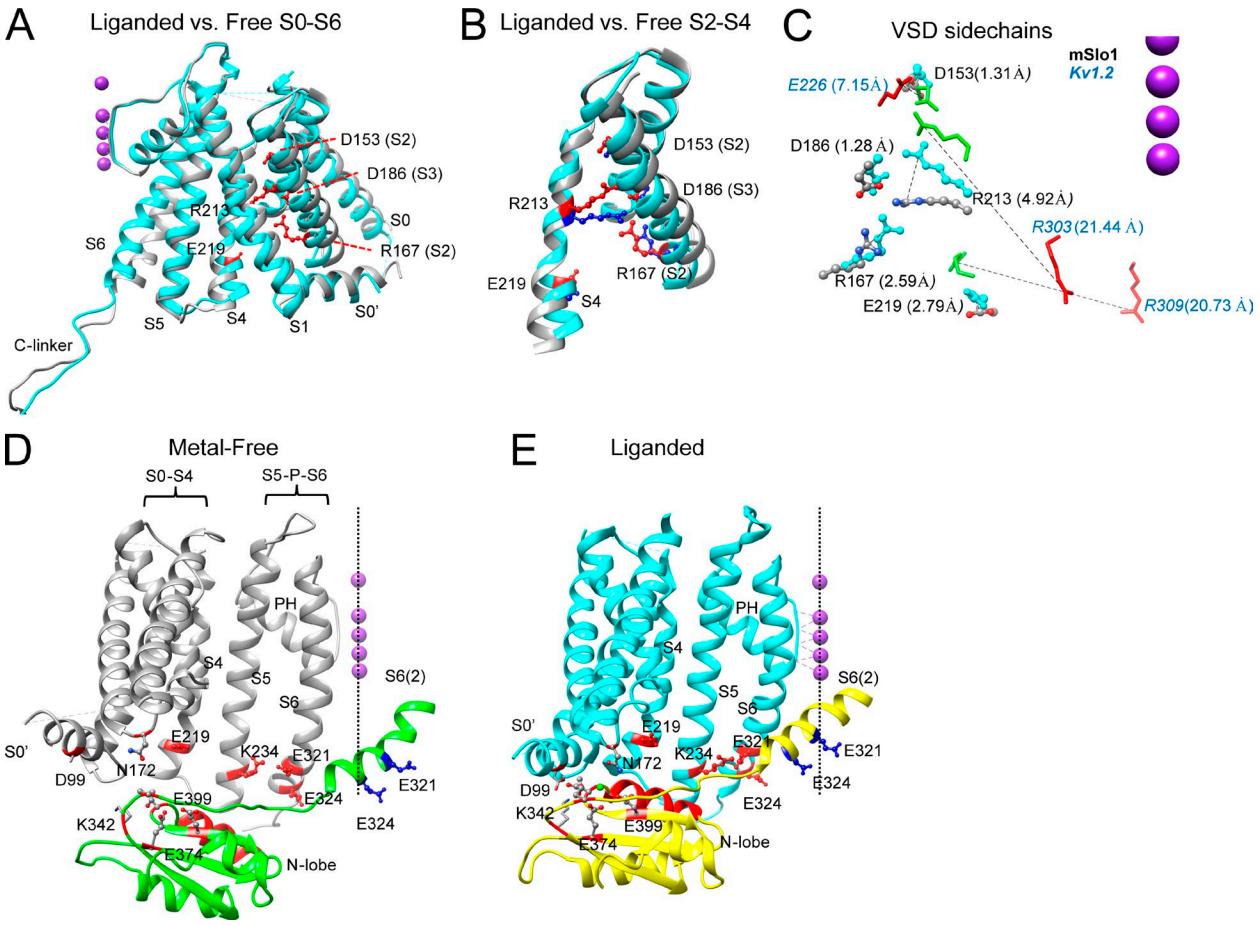


Figure 8. **Changes in VSD and VSD-RCK1 interactions with ligation.** (A) Comparison between liganded (cyan) and metal-free (gray) aSlo1 structures in the membrane-spanning domain for a single subunit. Structures were aligned such that selectivity filter and the pore helix (left of the structure) are superimposed. Side chains that contribute to gating charges (labeled with mSlo1 numbering) are shown in red ball-and-chains, with dotted lines helping identify some residues. S3 is hidden under S2. (B) Portion of A showing only S2, S3, and S4 for liganded (cyan) and metal-free (gray) structures, highlighting rather modest changes in VSD between structures. R213 corresponds to primary S4 gating charge residue. (C) Side chains of various mSlo1 (D153, D186, R167, R213, R219) and Kv1.2 (E226, R303, R309) implicated in voltage-sensing are shown for metal-free and liganded structures. Distance in angstroms is listed for net movement of charge center of given residue; dotted lines show vector of displacement for specific residues. Kv1.2 R309, although not a voltage-sensing residue, is shown to emphasize large extent of motion in S4 of Kv1.2. R213 in Slo1 and R303 of Kv1.2 correspond to the identical R4 position. The aSlo1 and Kv1.2 structures were aligned based on the selectivity filters, but the corresponding $K^+$ ion positions have been displaced closer to the S4 positions to minimize figure size. (D) Part of two adjacent subunits of the liganded aSlo1 structure are displayed, one (gray) showing S1–S6 and the other (green) showing part of S6 and N-lobe of RCK1. Residue labeling corresponds to mammalian sequence; mE219/aD208 and mR213/aR202 in S4, mK234/aR223 in S5, and mE321/mE324 (aE310/aE313) in the C-linker are shown in red in one subunit; mE321 and mE324 in the other subunit are shown in blue. Residues involved in $Mg^{2+}$ coordination are also shown, along with two residues (mD99/aD88 and mK342/aK331) that may stabilize an interaction between the TM domain and the N-lobe. Dotted vertical line highlights the pore axis along with $K^+$ ions (not part of structure). The αB helix of the N-lobe suggested to be involved in interactions with TM elements is also highlighted in red. (E) Liganded structures for the same elements shown in C are shown, showing the pronounced repositioning of the N-lobe of one subunit to allow interaction with the elements of the transmembrane domain. The S6 helix associated with the subunit containing the N-lobe appears to shift approximately one helical turn once the N-lobe interaction is stabilized. The panel highlights several potential domain interactions that may influence gating, including (1) interactions among S4–S5 with S6, (2) interactions among VSD and the S4–S5 linker with the N-lobe of RCK1, (3) interactions between mD99 and mK342, and (4) direct connection via the C-linker between the N-lobe of RCK1 and S6.

driving the difference in VSD position between the two aSlo1 structures, but the difference arises from ligation of divalent cation. Thus, whether the VSD position in the liganded channel reflects a position normally occurring with depolarization is uncertain. Second, it is uncertain whether the two resolved states represent conformations with, on one hand, fully resting VSDs and, on the other, fully active VSDs. Based on functional tests (Horrigan and Aldrich, 2002), at 0 mV in the absence of ligand, mSlo1 VSDs are expected to be largely in resting states. Thus, it seems reasonable that the metal-free structure may reflect the normal resting position of aSlo1 VSDs.

However, for the liganded structure, the situation is much less clear. To address this, we compared (Fig. 8 C) the extent of displacement of various voltage-sensing associated residues in the aSlo1 structures to those in models of closed and open Kv1.2 channels (Pathak et al., 2007). Several residues potentially implicated in Slo1 voltage sensing, including mD153, mD186, and mR167 (Ma et al., 2006), and also mE219 (Zhang et al., 2014), exhibit minimal change between the two structures, perhaps indicating that their effects on voltage sensing are indirect. Only mR213, in VSD position R4, exhibits appreciable change consistent with a 4.4-Å vertical displacement in the membrane field. In contrast, the R4 residue in Kv1.2 (R309) exhibits extensive motion between resting and activated models, with a 15.8-Å vertical displacement. Is the motion of Slo1 R213 likely to represent a full excursion of the Slo1 VSD between resting and active conformations? This certainly can't be answered definitively, but we point out two features of the structures. The metal-free positions of Slo1 mR213, along with the other putative Slo1 voltage-sensing side chains, are close to the positions of the corresponding residues in the activated Kv1.2 channel (Fig. 8 C). Furthermore, the fractional vertical displacement of Slo1 R213 compared with Kv1.2 R309 is 0.28, which is remarkably congruent with the ∼0.3-e charge movement of R213 in Slo1 relative to the ∼1-e charge movement for R4 residue in Shaker (Ma et al., 2006). Yet, although these factors might tend to argue that the liganded aSlo1 structure has fully active VSDs, this remains difficult to reconcile with the fact that, at nominal 0 mV, even with 70 µM $Ca^{2+}$, the fraction of VSDs in active positions is expected to be less than 0.2 (Horrigan and Aldrich, 2002). It may be possible that the presence of $Mg^{2+}$ produces an additional shift in the steady-state VSD equilibrium, but previous results are insufficient to address this (Horrigan and Ma, 2008). Overall, then, the question of whether VSDs in the liganded aSlo1 structure are representative of fully activated VSDs will require future attention. Yet clearly the new structures do show that the aSlo1 VSDs change position with ligation, and a key question becomes, what is the importance of these VSD changes in channel activation?

### How does VSD activation couple to Slo1 activation?

Based on functional tests, VSD movements are thought to open the activation gate in Slo1 channels via an allosteric mechanism: the gate can open in the absence of VSD activation, but VSD activation facilitates channel opening (Horrigan et al., 1999; Horrigan and Aldrich, 2002). For Slo1, a somewhat standard view of VSD-mediated channel activation, similar to VSD activation of Kv channels, has been that VSD activation directly influences PGD status (Horrigan and Aldrich, 2002). In accordance with this idea, movements of the VSD must be propagated to the pore to bias the conformational status of the pore. Numerous mutational studies have attempted to probe such interactions, identifying residues that shift or alter the steepness of voltage-dependent activation, but only a few residues have been identified as candidates to influence VSD–pore coupling. In one case, an interaction between mE219 and mE321/E324, located on the cytosolic side of S4 and S6, respectively, may contribute to VSD–pore coupling (Zhang et al., 2014). Mutations of mE219 shifted voltage dependence of both VSD activation and pore opening, and, in accordance with the allosteric model of voltage-dependent Slo1 activation (Horrigan et al., 1999; Horrigan and Aldrich, 2002), the results were consistent with a reduced VSD–pore coupling (Zhang et al., 2014). Mutations of mE180, mE186, and mR210 also were shown to produce effects consistent with a reduction in coupling energies between VSD and PGD (Ma et al., 2006). These results suggest that interactions between residues in different membrane-spanning segments can impact on VSD-pore coupling. Interestingly, for mutations of mE219, the results and analysis also suggested an enhanced $Ca^{2+}$-dependent activation, possibly by strengthening the coupling between $Ca^{2+}$ binding and pore opening (Zhang et al., 2014). This raised the possibility that some aspect of the VSD may influence coupling between $Ca^{2+}$ binding and pore.

The idea that the ability of the VSD to influence PGD activation may involve the CTD has been given additional support in other recent work. For example, use of the truncated mSlo1 (core-MT) construct lacking the CTD (Budelli et al., 2013) revealed that CTD removal produces only a modest −20-mV shift of the charge–voltage (Q-V) relation measured from gating current, but markedly reduces the strength of the VSD–pore coupling (Zhang et al., 2017). Specifically, activation of the VSD in the core-MT channels is 100-fold less effective at increasing channel Po compared with WT channels (Zhang et al., 2017). This removal of the CTD results in a 25% reduction in the free energy of the strength of VSD–core coupling. Interactions between VSD and CTD during Slo1 gating have also been revealed by results showing that $Ca^{2+}$ binding alters voltage dependence of gating charge movements (Horrigan and Aldrich, 2002; Savalli et al., 2012). Furthermore, fluorescence measurement of movements in the CTD during channel gating also showed voltage dependence (Miranda et al., 2013).

The new structures now provide a stronger basis for thinking about how VSD–CTD interactions may affect channel gating, and Hite et al. (2017) importantly focused attention on the importance of domain interactions, particularly between the VSD and the CTD, as conduits by which $Ca^{2+}/Mg^{2+}$ ligation may influence VSD status and vice versa. However, as pointed out in the previous section (Differences in the Slo1 VSD between metal-free and liganded structures), a limitation in assessing the significance of the changes in VSD be-

tween the two aSlo1 structures arises from uncertainty about the functional status of the VSD in each structure. This limitation is compounded by the fact that the structures still do not reveal what the basic change in the aSlo1 protein may be that distinguishes an open channel from a closed channel. In the absence of the latter information, it becomes only speculation about to the extent to which a particular movement of S4–S5 or a particular movement of the C-linker-S6 is critically linked to channel activation.

The unambiguous fact that the new structures point to defined physical linkages between the VSD and the CTD clearly represents a major step in thinking about how Slo1 channels are activated. But whether the observed VSD movement is critical for ligand-dependent channel activation is uncertain. Given the shift in the VSD equilibrium between 0 and 70 µM $Ca^{2+}$, it is possible that the change in VSD position with ligation simply reflects a structural change associated with that change in equilibrium, while not markedly increasing the fraction of "activated" VSDs when measured at 0 mV. This issue of how the various sensor domains couple to channel activation will remain central to work on BK channels and will benefit both from new biophysical work, and also additional structures. For example, an aSlo1 structure with $Mg^{2+}$-coordinating residues (e.g., mE399) mutated might help resolve whether any of the N-lobe motions are unique to $Mg^{2+}$ ligation or can occur with $Ca^{2+}$ alone. An aSlo1 structure with the mR210C or mR207Q mutation might be expected to have proteins with activated VSDs even at 0 mV (Ma et al., 2006). Such additional structures might help provide additional insight into how the status of particular sensor domains affects structural changes in other domains.

One of the major contributions of these new structures will be in how they guide thinking about domain–domain interactions. The perhaps traditional view of voltage activation of Kv channels is that interaction between the S4–S5 linker and the cytosolic side of S6 is proposed as the primary mechanism for the VSD–pore coupling (Lu et al., 2002; Tristani-Firouzi et al., 2002; Long et al., 2005b). In Slo1, the short length of the Slo1 S4–S5 linker may tend to preclude a similar mechanism. Probably the most remarkable structural difference between the two aSlo1 structures that might be expected to be associated with channel activation reflects the movement of the N-lobe region of the CTD in a fashion that allows formation of stabilizing interactions between the N-lobe residue mK342 (aK331) with mD99 (aD86) in the S0′ linker (Fig. 8, D and E). The original Figs. 3 and 4 in Hite et al. (2017) also nicely show these changes. The N-lobe/VSD interaction results in a displacement of the C-linker and the S6 helix attached to the N-lobe of about a full helical turn, consistent with the lateral motions of the S6 helices shown earlier in the videos. Based on these differences between the metal-free and liganded structures, Hite et al. (2017) suggested that both VSD–CTD interactions and N-lobe influences on C-linker-S6 are contributors to how ligation may lead to channel activation. Whether these N-lobe–VSD interactions also occur in the absence of $Mg^{2+}$ binding needs to be resolved.

Overall, the functional and structural results leave open several possibilities in regard to interactions that may be critical for mediating channel activation. First, it remains possible that tight packing between S4 and S5 might play an important role in VSD–pore coupling. For instance, the interaction between mE219 and mE321/mE324 observed in functional studies (Zhang et al., 2014) may be mediated by an intervening basic residue, mK234 in S5, which is located in the middle between mE219 and mE321/mE324 (Fig. 8, D and E). Second, as proposed by Hite et al. (2017) and just discussed, the VSD and S4-S5 linker may interact with the N-lobe of RCK1, thereby influencing PGD activation. As a corollary, it might be expected that VSD activation in response to voltage changes may also affect the interactions with the N-lobe of RCK1. That the VSD–PGD coupling may be mediated in part through the cytosolic gating ring (Hite et al., 2017) is perhaps consistent with the weakened VSD–pore coupling observed after removal of the cytosolic domain (Zhang et al., 2017). Overall, there are a variety of domain–domain interactions that may participate in regulation of Slo1 activation (Fig. 8, D and E). Together, the new structures pose several provocative ideas regarding the potential coupling of sensor domains to the PGD and point the way toward new functional and structural tests that will ultimately be required to answer the questions of how both voltage sensing and ligand binding participate in producing Slo1 channel activation.

## Concluding remarks

In summary, the new structures reveal the physical basis for several features of BK channels inferred from functional studies: (1) the large dimensions of the inner cavities of both a liganded, open channel and a metal-free, presumably nonconductive pore; (2) the identity of $Ca^{2+}$-coordinating residues in both RCK1 and RCK2; (3) the identity of $Mg^{2+}$-coordinating residues; (4) a different positioning of VSD to the PGD within a single Slo1 subunit compared with Kv, and (5) domain-swapping between VSD and CTD. The new structures raise several intriguing issues: (1) the possibility of an influence of the $Ca^{2+}$ occupancy of one binding site within one subunit on the $Ca^{2+}$ binding in the other site; and (2) a new perspective on how voltage sensing may affect the ability of the CTD to gate the BK channel. Issues that remain unanswered include (1) the absence of a clear structural basis for state-dependent accessibility changes, or the ability of particular mutations in S6 to shift gating; (2) the location of the gate to ion perme-

ation, (3) a clear correlation between structures and functional states, and (4) clear answers to the challenging questions of how VSD or CTD activation couples to channel openings.

Although it is likely that the $Ca^{2+}/Mg^{2+}$ liganded channel represents a fully activated conformation, to what extent this is similar to a liganded channel in the absence of $Mg^{2+}$ is unknown. Furthermore, the functional correlate of the metal-free structure is somewhat uncertain. The gating ring structures for both the liganded and metal-free structures correspond very well with the liganded and apo-states of the isolated gating ring structures. Given that at nominal 0 mV, Slo1 voltage sensors are predominantly in resting states in a metal-free condition, it would be expected that the metal-free structure would be fully closed. However, uncertainty about whether the metal-free structure can explain some of the functional features expected for a closed channel keeps open some uncertainty about what functional state it represents. From this perspective, additional work will be required to resolve this issue, and any conclusions regarding changes in the PGD or VSD that occur during gating must be tempered by that uncertainty.

### Online supplemental material

Video 1 shows animation (view from the cytosol) of interpolated movement between metal-free and liganded aSlo1 structures (Hite et al., 2017; Tao et al., 2017). Video 2 shows side-view animation of interpolated movement between metal-free and liganded aSlo1 structures. Video 3 shows animation (view from the cytosol) of interpolated movement between closed and open Kv1.2 based on two published structural models from Pathak et al. (2007), with the structures aligned based on selectivity filter and pore helix. Video 4 shows side-view animation of interpolated movement between closed and open Kv1.2 model structures.

## ACKNOWLEDGMENTS

We thank Drs. Guohui Zhang and Zhiguang Jia for help in making Fig. 8.

This review is supported by National Institutes of Health grants HL70393 and GM114694 (to J. Cui), NS086916 (to H. Yang), and GM118114 (to C.J. Lingle).

The authors declare no competing financial interests.

Lesley C. Anson served as editor.

Submitted: 6 July 2017
Accepted: 20 September 2017

## REFERENCES

Ahmad, S., M. Gromiha, H. Fawareh, and A. Sarai. 2004. ASAView: Database and tool for solvent accessibility representation in proteins. *BMC Bioinformatics.* 5:51. https://doi.org/10.1186/1471-2105-5-51

Aryal, P., F. Abd-Wahab, G. Bucci, M.S. Sansom, and S.J. Tucker. 2014. A hydrophobic barrier deep within the inner pore of the TWIK-1 K2P potassium channel. *Nat. Commun.* 5:4377. https://doi.org/10.1038/ncomms5377

Bao, L., A.M. Rapin, E.C. Holmstrand, and D.H. Cox. 2002. Elimination of the $BK_{Ca}$ channel's high-affinity $Ca^{2+}$ sensitivity. *J. Gen. Physiol.* 120:173–189. https://doi.org/10.1085/jgp.20028627

Bao, L., C. Kaldany, E.C. Holmstrand, and D.H. Cox. 2004. Mapping the $BK_{Ca}$ channel's "$Ca^{2+}$ bowl". *J. Gen. Physiol.* 123:475–489. https://doi.org/10.1085/jgp.200409052

Bian, S., I. Favre, and E. Moczydlowski. 2001. $Ca^{2+}$-binding activity of a COOH-terminal fragment of the Drosophila BK channel involved in $Ca^{2+}$-dependent activation. *Proc. Natl. Acad. Sci. USA.* 98:4776–4781. https://doi.org/10.1073/pnas.081072398

Brelidze, T.I., and K.L. Magleby. 2005. Probing the geometry of the inner vestibule of BK channels with sugars. *J. Gen. Physiol.* 126:105–121. https://doi.org/10.1085/jgp.200509286

Brinley, F.J. Jr., A. Scarpa, and T. Tiffert. 1977. The concentration of ionized magnesium in barnacle muscle fibres. *J. Physiol.* 266:545–565. https://doi.org/10.1113/jphysiol.1977.sp011781

Bruening-Wright, A., M.A. Schumacher, J.P. Adelman, and J. Maylie. 2002. Localization of the activation gate for small conductance $Ca^{2+}$-activated $K^+$ channels. *J. Neurosci.* 22:6499–6506.

Budelli, G., Y. Geng, A. Butler, K.L. Magleby, and L. Salkoff. 2013. Properties of Slo1 $K^+$ channels with and without the gating ring. *Proc. Natl. Acad. Sci. USA.* 110:16657–16662. https://doi.org/10.1073/pnas.1313433110

Cao, Y., Y. Pan, H. Huang, X. Jin, E.J. Levin, B. Kloss, and M. Zhou. 2013. Gating of the TrkH ion channel by its associated RCK protein TrkA. *Nature.* 496:317–322. https://doi.org/10.1038/nature12056

Chen, X., and R.W. Aldrich. 2011. Charge substitution for a deep-pore residue reveals structural dynamics during BK channel gating. *J. Gen. Physiol.* 138:137–154. https://doi.org/10.1085/jgp.201110632

Chen, R.S., Y. Geng, and K.L. Magleby. 2011. $Mg^{2+}$ binding to open and closed states can activate BK channels provided that the voltage sensors are elevated. *J. Gen. Physiol.* 138:593–607. https://doi.org/10.1085/jgp.201110707

Chen, X., J. Yan, and R.W. Aldrich. 2014. BK channel opening involves side-chain reorientation of multiple deep-pore residues. *Proc. Natl. Acad. Sci. USA.* 111:E79–E88. https://doi.org/10.1073/pnas.1321697111

Contreras, J.E., D. Srikumar, and M. Holmgren. 2008. Gating at the selectivity filter in cyclic nucleotide-gated channels. *Proc. Natl. Acad. Sci. USA.* 105:3310–3314. https://doi.org/10.1073/pnas.0709809105

Cox, D.H., J. Cui, and R.W. Aldrich. 1997. Allosteric gating of a large conductance Ca-activated $K^+$ channel. *J. Gen. Physiol.* 110:257–281. https://doi.org/10.1085/jgp.110.3.257

Cui, J., D.H. Cox, and R.W. Aldrich. 1997. Intrinsic voltage dependence and $Ca^{2+}$ regulation of *mslo* large conductance Ca-activated $K^+$ channels. *J. Gen. Physiol.* 109:647–673. https://doi.org/10.1085/jgp.109.5.647

del Camino, D., and G. Yellen. 2001. Tight steric closure at the intracellular activation gate of a voltage-gated K(+) channel. *Neuron.* 32:649–656. https://doi.org/10.1016/S0896-6273(01)00487-1

Díaz, L., P. Meera, J. Amigo, E. Stefani, O. Alvarez, L. Toro, and R. Latorre. 1998. Role of the S4 segment in a voltage-dependent calcium-sensitive potassium (hSlo) channel. *J. Biol. Chem.* 273:32430–32436. https://doi.org/10.1074/jbc.273.49.32430

Ding, S., L. Ingleby, C.A. Ahern, and R. Horn. 2005. Investigating the putative glycine hinge in Shaker potassium channel. *J. Gen. Physiol.* 126:213–226. https://doi.org/10.1085/jgp.200509287

Doyle, D.A., J. Morais Cabral, R.A. Pfuetzner, A. Kuo, J.M. Gulbis, S.L. Cohen, B.T. Chait, and R. MacKinnon. 1998. The structure of the potassium channel: Molecular basis of $K^+$ conduction and selectivity. *Science.* 280:69–77. https://doi.org/10.1126/science.280.5360.69

Garg, P., A. Gardner, V. Garg, and M.C. Sanguinetti. 2013. Structural basis of ion permeation gating in Slo2.1 $K^+$ channels. *J. Gen. Physiol.* 142:523–542. https://doi.org/10.1085/jgp.201311064

Geng, Y., X. Niu, and K.L. Magleby. 2011. Low resistance, large dimension entrance to the inner cavity of BK channels determined by changing side-chain volume. *J. Gen. Physiol.* 137:533–548. https://doi.org/10.1085/jgp.201110616

Golowasch, J., A. Kirkwood, and C. Miller. 1986. Allosteric effects of $Mg^{2+}$ on the gating of $Ca^{2+}$-activated $K^+$ channels from mammalian skeletal muscle. *J. Exp. Biol.* 124:5–13.

Hite, R.K., X. Tao, and R. MacKinnon. 2017. Structural basis for gating the high-conductance $Ca^{2+}$-activated $K^+$ channel. *Nature.* 541:52–57. https://doi.org/10.1038/nature20775

Horrigan, F.T., and R.W. Aldrich. 1999. Allosteric voltage gating of potassium channels II. *J. Gen. Physiol.* 114:305–336. https://doi.org/10.1085/jgp.114.2.305

Horrigan, F.T., and R.W. Aldrich. 2002. Coupling between voltage sensor activation, $Ca^{2+}$ binding and channel opening in large conductance (BK) potassium channels. *J. Gen. Physiol.* 120:267–305. https://doi.org/10.1085/jgp.20028605

Horrigan, F.T., and Z. Ma. 2008. $Mg^{2+}$ enhances voltage sensor/gate coupling in BK channels. *J. Gen. Physiol.* 131:13–32. https://doi.org/10.1085/jgp.200709877

Horrigan, F.T., J. Cui, and R.W. Aldrich. 1999. Allosteric voltage gating of potassium channels I. *J. Gen. Physiol.* 114:277–304. https://doi.org/10.1085/jgp.114.2.277

Hu, L., J. Shi, Z. Ma, G. Krishnamoorthy, F. Sieling, G. Zhang, F.T. Horrigan, and J. Cui. 2003. Participation of the S4 voltage sensor in the $Mg^{2+}$-dependent activation of large conductance (BK) $K^+$ channels. *Proc. Natl. Acad. Sci. USA.* 100:10488–10493. https://doi.org/10.1073/pnas.1834300100

Jiang, Y., A. Pico, M. Cadene, B.T. Chait, and R. MacKinnon. 2001. Structure of the RCK domain from the E. coli $K^+$ channel and demonstration of its presence in the human BK channel. *Neuron.* 29:593–601. https://doi.org/10.1016/S0896-6273(01)00236-7

Jiang, Y., A. Lee, J. Chen, M. Cadene, B.T. Chait, and R. MacKinnon. 2002a. Crystal structure and mechanism of a calcium-gated potassium channel. *Nature.* 417:515–522. https://doi.org/10.1038/417515a

Jiang, Y., A. Lee, J. Chen, M. Cadene, B.T. Chait, and R. MacKinnon. 2002b. The open pore conformation of potassium channels. *Nature.* 417:523–526. https://doi.org/10.1038/417523a

Koval, O.M., Y. Fan, and B.S. Rothberg. 2007. A role for the S0 transmembrane segment in voltage-dependent gating of BK channels. *J. Gen. Physiol.* 129:209–220. https://doi.org/10.1085/jgp.200609662

Krishnamoorthy, G., J. Shi, D. Sept, and J. Cui. 2005. The $NH_2$ terminus of RCK1 domain regulates $Ca^{2+}$-dependent $BK_{Ca}$ channel gating. *J. Gen. Physiol.* 126:227–241. https://doi.org/10.1085/jgp.200509321

Lee, U.S., J. Shi, and J. Cui. 2010. Modulation of BK channel gating by the β2 subunit involves both membrane-spanning and cytoplasmic domains of Slo1. *J. Neurosci.* 30:16170–16179. https://doi.org/10.1523/JNEUROSCI.2323-10.2010

Lenaeus, M.J., M. Vamvouka, P.J. Focia, and A. Gross. 2005. Structural basis of TEA blockade in a model potassium channel. *Nat. Struct. Mol. Biol.* 12:454–459. https://doi.org/10.1038/nsmb929

Li, W., and R.W. Aldrich. 2004. Unique inner pore properties of BK channels revealed by quaternary ammonium block. *J. Gen. Physiol.* 124:43–57. https://doi.org/10.1085/jgp.200409067

Li, W., and R.W. Aldrich. 2006. State-dependent block of BK channels by synthesized shaker ball peptides. *J. Gen. Physiol.* 128:423–441. https://doi.org/10.1085/jgp.200609521

Lingle, C.J. 2007. Gating rings formed by RCK domains: Keys to gate opening. *J. Gen. Physiol.* 129:101–107. https://doi.org/10.1085/jgp.200709739

Liu, G., S.I. Zakharov, L. Yang, S.X. Deng, D.W. Landry, A. Karlin, and S.O. Marx. 2008. Position and role of the BK channel α subunit S0 helix inferred from disulfide crosslinking. *J. Gen. Physiol.* 131:537–548. https://doi.org/10.1085/jgp.200809968

Liu, Y., M. Holmgren, M.E. Jurman, and G. Yellen. 1997. Gated access to the pore of a voltage-dependent $K^+$ channel. *Neuron.* 19:175–184. https://doi.org/10.1016/S0896-6273(00)80357-8

Long, S.B., E.B. Campbell, and R. Mackinnon. 2005a. Crystal structure of a mammalian voltage-dependent Shaker family $K^+$ channel. *Science.* 309:897–903. https://doi.org/10.1126/science.1116269

Long, S.B., E.B. Campbell, and R. Mackinnon. 2005b. Voltage sensor of Kv1.2: Structural basis of electromechanical coupling. *Science.* 309:903–908. https://doi.org/10.1126/science.1116270

Long, S.B., X. Tao, E.B. Campbell, and R. MacKinnon. 2007. Atomic structure of a voltage-dependent $K^+$ channel in a lipid membrane-like environment. *Nature.* 450:376–382. https://doi.org/10.1038/nature06265

Lu, Z., A.M. Klem, and Y. Ramu. 2002. Coupling between voltage sensors and activation gate in voltage-gated $K^+$ channels. *J. Gen. Physiol.* 120:663–676. https://doi.org/10.1085/jgp.20028696

Ma, Z., X.J. Lou, and F.T. Horrigan. 2006. Role of charged residues in the S1-S4 voltage sensor of BK channels. *J. Gen. Physiol.* 127:309–328. https://doi.org/10.1085/jgp.200509421

Ma, Z., K.Y. Wong, and F.T. Horrigan. 2008. An extracellular $Cu^{2+}$ binding site in the voltage sensor of BK and Shaker potassium channels. *J. Gen. Physiol.* 131:483–502. https://doi.org/10.1085/jgp.200809980

McManus, O.B., and K.L. Magleby. 1991. Accounting for the Ca(2+)-dependent kinetics of single large-conductance Ca(2+)-activated $K^+$ channels in rat skeletal muscle. *J. Physiol.* 443:739–777. https://doi.org/10.1113/jphysiol.1991.sp018861

Meera, P., M. Wallner, M. Song, and L. Toro. 1997. Large conductance voltage- and calcium-dependent $K^+$ channel, a distinct member of voltage-dependent ion channels with seven N-terminal transmembrane segments (S0-S6), an extracellular N terminus, and an intracellular (S9-S10) C terminus. *Proc. Natl. Acad. Sci. USA.* 94:14066–14071. https://doi.org/10.1073/pnas.94.25.14066

Miranda, P., J.E. Contreras, A.J. Plested, F.J. Sigworth, M. Holmgren, and T. Giraldez. 2013. State-dependent FRET reports calcium- and voltage-dependent gating-ring motions in BK channels. *Proc. Natl. Acad. Sci. USA.* 110:5217–5222. https://doi.org/10.1073/pnas.1219611110

Niu, X., X. Qian, and K.L. Magleby. 2004. Linker-gating ring complex as passive spring and Ca(2+)-dependent machine for a voltage- and Ca(2+)-activated potassium channel. *Neuron.* 42:745–756. https://doi.org/10.1016/j.neuron.2004.05.001

Oberhauser, A., O. Alvarez, and R. Latorre. 1988. Activation by divalent cations of a $Ca^{2+}$-activated $K^+$ channel from skeletal muscle membrane. *J. Gen. Physiol.* 92:67–86. https://doi.org/10.1085/jgp.92.1.67

Pantazis, A., V. Gudzenko, N. Savalli, D. Sigg, and R. Olcese. 2010. Operation of the voltage sensor of a human voltage- and $Ca^{2+}$-activated $K^+$ channel. *Proc. Natl. Acad. Sci. USA.* 107:4459–4464. https://doi.org/10.1073/pnas.0911959107

Pathak, M.M., V. Yarov-Yarovoy, G. Agarwal, B. Roux, P. Barth, S. Kohout, F. Tombola, and E.Y. Isacoff. 2007. Closing in on the resting state of the Shaker K(+) channel. *Neuron.* 56:124–140. https://doi.org/10.1016/j.neuron.2007.09.023

Posson, D.J., J.G. McCoy, and C.M. Nimigean. 2013. The voltage-dependent gate in MthK potassium channels is located at the selectivity filter. *Nat. Struct. Mol. Biol.* 20:159–166. https://doi.org/10.1038/nsmb.2473

Posson, D.J., R. Rusinova, O.S. Andersen, and C.M. Nimigean. 2015. Calcium ions open a selectivity filter gate during activation of the MthK potassium channel. *Nat. Commun.* 6:8342. https://doi.org/10.1038/ncomms9342

Prosser, C.L. 1973. Comparative Animal Physiology. Third edition. Saunders, Philadelphia.

Qian, X., X. Niu, and K.L. Magleby. 2006. Intra- and intersubunit cooperativity in activation of BK channels by $Ca^{2+}$. *J. Gen. Physiol.* 128:389–404. https://doi.org/10.1085/jgp.200609486

Roth, R., D. Gillespie, W. Nonner, and R.E. Eisenberg. 2008. Bubbles, gating, and anesthetics in ion channels. *Biophys. J.* 94:4282–4298. https://doi.org/10.1529/biophysj.107.120493

Rothberg, B.S. 2012. The BK channel: A vital link between cellular calcium and electrical signaling. *Protein Cell.* 3:883–892. https://doi.org/10.1007/s13238-012-2076-8

Rothberg, B.S., and K.L. Magleby. 2000. Voltage and $Ca^{2+}$ activation of single large-conductance $Ca^{2+}$-activated $K^+$ channels described by a two-tiered allosteric gating mechanism. *J. Gen. Physiol.* 116:75–99. https://doi.org/10.1085/jgp.116.1.75

Savalli, N., A. Pantazis, T. Yusifov, D. Sigg, and R. Olcese. 2012. The contribution of RCK domains to human BK channel allosteric activation. *J. Biol. Chem.* 287:21741–21750. https://doi.org/10.1074/jbc.M112.346171

Schreiber, M., and L. Salkoff. 1997. A novel calcium-sensing domain in the BK channel. *Biophys. J.* 73:1355–1363. https://doi.org/10.1016/S0006-3495(97)78168-2

Schreiber, M., A. Wei, A. Yuan, J. Gaut, M. Saito, and L. Salkoff. 1998. Slo3, a novel pH-sensitive $K^+$ channel from mammalian spermatocytes. *J. Biol. Chem.* 273:3509–3516. https://doi.org/10.1074/jbc.273.6.3509

Schreiber, M., A. Yuan, and L. Salkoff. 1999. Transplantable sites confer calcium sensitivity to BK channels. *Nat. Neurosci.* 2:416–421. https://doi.org/10.1038/8077

Shi, J., and J. Cui. 2001. Intracellular $Mg^{2+}$ enhances the function of BK-type $Ca^{2+}$-activated $K^+$ channels. *J. Gen. Physiol.* 118:589–606. https://doi.org/10.1085/jgp.118.5.589

Shi, J., G. Krishnamoorthy, Y. Yang, L. Hu, N. Chaturvedi, D. Harilal, J. Qin, and J. Cui. 2002. Mechanism of magnesium activation of calcium-activated potassium channels. *Nature.* 418:876–880. https://doi.org/10.1038/nature00941

Stefani, E., M. Ottolia, F. Noceti, R. Olcese, M. Wallner, R. Latorre, and L. Toro. 1997. Voltage-controlled gating in a large conductance $Ca^{2+}$-sensitive $K^+$channel (hslo). *Proc. Natl. Acad. Sci. USA.* 94:5427–5431. https://doi.org/10.1073/pnas.94.10.5427

Sweet, T.B., and D.H. Cox. 2008. Measurements of the BKCa channel's high-affinity $Ca^{2+}$ binding constants: Effects of membrane voltage. *J. Gen. Physiol.* 132:491–505. https://doi.org/10.1085/jgp.200810094

Tang, Q.Y., X.H. Zeng, and C.J. Lingle. 2009. Closed-channel block of BK potassium channels by bbTBA requires partial activation. *J. Gen. Physiol.* 134:409–436. https://doi.org/10.1085/jgp.200910251

Tao, X., R.K. Hite, and R. MacKinnon. 2017. Cryo-EM structure of the open high-conductance $Ca^{2+}$-activated $K^+$ channel. *Nature.* 541:46–51. https://doi.org/10.1038/nature20608

Thompson, J., and T. Begenisich. 2012. Selectivity filter gating in large-conductance $Ca^{2+}$-activated $K^+$ channels. *J. Gen. Physiol.* 139:235–244. https://doi.org/10.1085/jgp.201110748

Tristani-Firouzi, M., J. Chen, and M.C. Sanguinetti. 2002. Interactions between S4-S5 linker and S6 transmembrane domain modulate gating of HERG $K^+$ channels. *J. Biol. Chem.* 277:18994–19000. https://doi.org/10.1074/jbc.M200410200

Wilkens, C.M., and R.W. Aldrich. 2006. State-independent block of BK channels by an intracellular quaternary ammonium. *J. Gen. Physiol.* 128:347–364. https://doi.org/10.1085/jgp.200609579

Wu, Y., Y. Yang, S. Ye, and Y. Jiang. 2010. Structure of the gating ring from the human large-conductance Ca(2+)-gated K(+) channel. *Nature.* 466:393–397. https://doi.org/10.1038/nature09252

Xia, X.M., X. Zeng, and C.J. Lingle. 2002. Multiple regulatory sites in large-conductance calcium-activated potassium channels. *Nature.* 418:880–884. https://doi.org/10.1038/nature00956

Xia, X.M., X. Zhang, and C.J. Lingle. 2004. Ligand-dependent activation of Slo family channels is defined by interchangeable cytosolic domains. *J. Neurosci.* 24:5585–5591. https://doi.org/10.1523/JNEUROSCI.1296-04.2004

Yang, H., and J. Cui. 2015. BK channels. *In* Handbook of Ion Channels. J. Zheng, and C. Mattew, editors. CRC Press, Boca Raton, FL. 227–240. https://doi.org/10.1201/b18027-21

Yang, H., L. Hu, J. Shi, K. Delaloye, F.T. Horrigan, and J. Cui. 2007. $Mg^{2+}$ mediates interaction between the voltage sensor and cytosolic domain to activate BK channels. *Proc. Natl. Acad. Sci. USA.* 104:18270–18275. https://doi.org/10.1073/pnas.0705873104

Yang, H., J. Shi, G. Zhang, J. Yang, K. Delaloye, and J. Cui. 2008. Activation of Slo1 BK channels by $Mg^{2+}$ coordinated between the voltage sensor and RCK1 domains. *Nat. Struct. Mol. Biol.* 15:1152–1159. https://doi.org/10.1038/nsmb.1507

Yang, H., G. Zhang, and J. Cui. 2015. BK channels: Multiple sensors, one activation gate. *Front. Physiol.* 6:29. https://doi.org/10.3389/fphys.2015.00029

Yang, J., G. Krishnamoorthy, A. Saxena, G. Zhang, J. Shi, H. Yang, K. Delaloye, D. Sept, and J. Cui. 2010. An epilepsy/dyskinesia-associated mutation enhances BK channel activation by potentiating $Ca^{2+}$ sensing. *Neuron.* 66:871–883. https://doi.org/10.1016/j.neuron.2010.05.009

Yang, J., H. Yang, X. Sun, K. Delaloye, X. Yang, A. Moller, J. Shi, and J. Cui. 2013. Interaction between residues in the $Mg^{2+}$-binding site regulates BK channel activation. *J. Gen. Physiol.* 141:217–228. https://doi.org/10.1085/jgp.201210794

Yuan, P., M.D. Leonetti, A.R. Pico, Y. Hsiung, and R. MacKinnon. 2010. Structure of the human BK channel $Ca^{2+}$-activation apparatus at 3.0 A resolution. *Science.* 329:182–186. https://doi.org/10.1126/science.1190414

Yuan, P., M.D. Leonetti, Y. Hsiung, and R. MacKinnon. 2011. Open structure of the Ca2+ gating ring in the high-conductance Ca2+-activated K+ channel. *Nature.* 481:94–97. https://doi.org/10.1038/nature10670

Zeng, X.H., X.M. Xia, and C.J. Lingle. 2005. Divalent cation sensitivity of BK channel activation supports the existence of three distinct binding sites. *J. Gen. Physiol.* 125:273–286. https://doi.org/10.1085/jgp.200409239

Zhang, G., S.Y. Huang, J. Yang, J. Shi, X. Yang, A. Moller, X. Zou, and J. Cui. 2010. Ion sensing in the RCK1 domain of BK channels. *Proc. Natl. Acad. Sci. USA.* 107:18700–18705. https://doi.org/10.1073/pnas.1010124107

Zhang, G., H. Yang, H. Liang, J. Yang, J. Shi, K. McFarland, Y. Chen, and J. Cui. 2014. A charged residue in S4 regulates coupling among the activation gate, voltage, and $Ca^{2+}$ sensors in BK channels. *J. Neurosci.* 34:12280–12288. https://doi.org/10.1523/JNEUROSCI.1174-14.2014

Zhang, G., Y. Geng, Y. Jin, J. Shi, K. McFarland, K.L. Magleby, L. Salkoff, and J. Cui. 2017. Deletion of cytosolic gating ring decreases gate and voltage sensor coupling in BK channels. *J. Gen. Physiol.* 149:373–387. https://doi.org/10.1085/jgp.201611646

Zhang, X., C.R. Solaro, and C.J. Lingle. 2001. Allosteric regulation of BK channel gating by $Ca^{2+}$ and $Mg^{2+}$ through a nonselective, low affinity divalent cation site. *J. Gen. Physiol.* 118:607–636. https://doi.org/10.1085/jgp.118.5.607

Zhou, Y., X.M. Xia, and C.J. Lingle. 2011. Cysteine scanning and modification reveal major differences between BK channels and Kv channels in the inner pore region. *Proc. Natl. Acad. Sci. USA.* 108:12161–12166. https://doi.org/10.1073/pnas.1104150108

Zhou, Y., X.H. Zeng, and C.J. Lingle. 2012. Barium ions selectively activate BK channels via the $Ca^{2+}$-bowl site. *Proc. Natl. Acad. Sci. USA.* 109:11413–11418. https://doi.org/10.1073/pnas.1204444109

Zhou, Y., X.M. Xia, and C.J. Lingle. 2015. Cadmium-cysteine coordination in the BK inner pore region and its structural and functional implications. *Proc. Natl. Acad. Sci. USA.* 112:5237–5242. https://doi.org/10.1073/pnas.1500953112